AD NUMBER
AD848420
NEW LIMITATION CHANGE
TO Approved for public release, distribution unlimited
FROM Distribution authorized to U.S. Gov't. agencies and their contractors; Administrative/Operational Use; DEC 1968. Other requests shall be referred to Naval Air Weapons Center, Technical Library, China Lake, CA 93555-6100. Export Control.
AUTHORITY
usnwc ltr 30 aug 1974

NWC TP 4565

LOW-FREQUENCY COMBUSTION INSTABILITY PROGRESS REPORT 1 OCTOBER 1967—31 MARCH 1968

by

H. B. Mathes
T. L. Boggs
G. L. Dehority
J. E. Crump

Research Department

ABSTRACT. This semiannual report summarizes studies of the burning rate of composite propellants, acoustic and nonacoustic low-frequency combustion instability of composite propellants and nonisentropic combustion behavior in T-burners.

NAVAL WEAPONS CENTER
CHINA LAKE, CALIFORNIA * DECEMBER 1968

48

CONTENTS

Nomenclature iv

1. Introduction 1

2. Steady-State Combustion. 1
   2.1. Introduction 1
   2.2. Experimental Techniques 2
   2.3. Results and Discussion 3
   2.4. Comparison with Analytical Models. 9
   2.5. Conclusion and Implications for Future Work. 12

3. Nonacoustic Combustion Instability 13
   3.1. Introduction 13
   3.2. Layer-Frequency Concept. 13
   3.3. Recent Experimental Results. 14
   3.4. Summary and Implications for Future Work 17

4. Acoustic Instability 18

Appendixes:
   A. Nonacoustic Instability Data for A-167, A-168, and A-170 Propellants. 21
   B. Computer Program for Predictions of Gas Behavior in T-Burner . 29
   C. Sample of Typical Computer Output. 38

References 41

NOMENCLATURE

D	Diameter
L*	Characteristic length of chamber (free volume divided by nozzle throat area)
$\bar{M}$	Dimensionless mean gas velocity
T	Temperature
T'	Temperature perturbation
a	Acoustic wave velocity; constant in GDF theory
b	Constant in GDF theory
c	Constant in steady-state burning law, $r = cp^n$
n	Pressure exponent in steady-state burning rate law, $r = cp^n$, also acoustic wave mode number
p	Pressure
p'	Pressure perturbation
r	Burning rate
x	Dimensionless displacement
β	Phase between pressure and reference plane temperature
ε, ε_p	Ratio of maximum pressure perturbation to mean pressure
ε_T	Isentropicity parameter ($\varepsilon_T = 1$ for isentropic processes, $\varepsilon_T = 0$ for isothermal processes)
τ	Characteristic time to burn through a particle
ψ	Phase between pressure and emergence of element of gas from the combustion zone

SUBSCRIPTS

g	Gas
p	Pressure
T	Isentropicity
S	Reference surface

1. INTRODUCTION

The research described in this report is part of a continuing program (Ref. 1 and 2) of investigation of the processes involved in acoustic and nonacoustic low-frequency combustion instability behavior of solid-propellant rocket motors and in various aspects of steady-state combustion believed to be related to combustion instability. Accompanying work on the deflagration of ammonium perchlorate has been recently reported (Ref. 3).

This report is divided into three parts. The first part gives the strand burning rates of the various propellants used in the combustion instability studies, compares the results with the granular diffusion flame theory, and points out the need for a more thorough examination of the burning-rate—pressure relationship assumed for the mathematical models of combustion instability. The second part presents additional experimental data on nonacoustic instability for propellants using a carboxy-terminated polybutadiene binder; these data like those obtained from polyurethane binder propellants ~~(Ref. 1 and 2)~~ also deviate from the one-dimensional theory. The third part of the report presents an extended mathematical description of nonisentropic behavior in the T-burner and compares experimental observations of the gas motion and temperature with theoretical predictions.

2. STEADY-STATE COMBUSTION

2.1 INTRODUCTION

Knowledge of the pressure dependence of the burning rate of a solid propellant is necessary in order to make predictions of the combustion stability using currently available theories. To obtain this information for the propellants being used in the combustion instability studies and to perhaps gain further insight into the steady-state-combustion processes of composite propellants, a detailed determination of the strand burning rate of these propellants was made. This section presents the data for two classes of propellants: a series of ammonium perchlorate (AP) and polyurethane (PU) propellants, and a series composed of AP and carboxy-terminated polybutadiene (CTPB). The formulations tested are given in Table 2.1.

TABLE 2.1. Composition of Research Propellants

Propellant designation	Ingredients and weight percent			
	Ammonium Perchlorate		Binder	Other
A-146	37.5% 15μ	37.5% 80μ	25% polyurethane	....
A-148	37.0% 15μ	37.0% 200μ	25% polyurethane	1% carbon black
A-149	37.0% 90μ	37.0% 600μ	25% polyurethane	1% carbon black
A-151	37.0% 45μ	37.0% 200μ	25% polyurethane	1% carbon black
A-155	37.0% 45μ	37.0% 400μ	25% polyurethane	1% carbon black
A-156	51.8% 15μ	22.2% 200μ	25% polyurethane	1% carbon black
A-157	22.2% 15μ	51.8% 200μ	25% polyurethane	1% carbon black
A-158	37.2% 90μ	37.5% 600μ	25% polyurethane	....
A-159	36.0% 15μ	36.0% 200μ	25% polyurethane	1% carbon black 1% n-butyl ferrocene
A-160	36.0% 45μ	36.0% 400μ	25% polyurethane	1% carbon black 1% n-butyl ferrocene
A-167	37.0% 15μ	37.0% 80μ	25% CTPB	1% carbon black
A-168	37.0% 15μ	37.0% 200μ	25% CTPB	1% carbon black
A-169	37.0% 90μ	37.0% 600μ	25% CTPB	1% carbon black
A-170	37.0% 45μ	37.0% 200μ	25% CTPB	1% carbon black
A-171	37.0% 45μ	37.0% 400μ	25% CTPB	1% carbon black
A-172	51.8% 15μ	22.2% 200μ	25% CTPB	1% carbon black

2.2 EXPERIMENTAL TECHNIQUES

The samples used were 1/4- by 1/4- by 2-inch strands and were mounted in the combustion bomb (Ref. 1) and ignited by a 10-mil heated Nichrome wire. Two different systems were used to detect the regressing surface: the conventional fuze wire approach (Fig. 2.1a) and a technique, developed at this Center, which optically detects the burning surface (Fig. 2.1b).

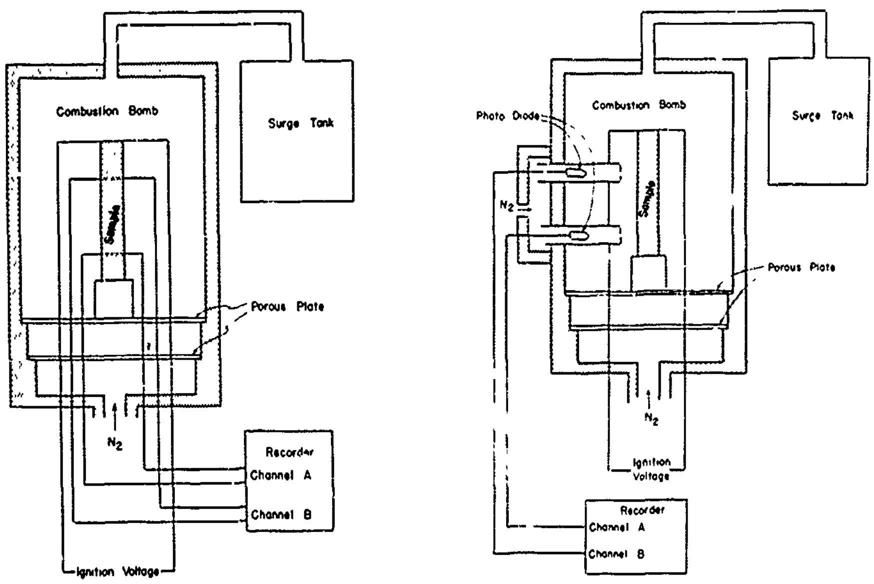

(a) (b)

FIG. 2.1. Burning Rate Apparatus. (a) Conventional strand burner, (b) NWC photodiode device.

This new apparatus utilizes photodiodes placed behind slit apertures to detect light emission as the burning surface passes the aperture. This technique has the advantages of (1) presenting no discontinuities (fuze wires, thermocouples, etc.) to the combustion front, (2) requiring no inhibiting of the samples, and (3) being able to detect a burning surface which is not normal to the strand axis. Data obtained from these two methods are in good agreement; further comparison with the rate calculated from high speed cinephotomicrography indicates that the photodiode method gives a rate slightly more consistent with that obtained from the motion pictures.

2.3 RESULTS AND DISCUSSION

The burning-rate curves are presented for the PU propellants (Fig. 2.2-2.11) and the CTPB propellants (Fig. 2.12-2.17). Each data point represents one burning rate test. In looking first at the combined plot (Fig. 2.2) which gives most of the burning rates for the polyurethanes, several features are discernible. The first observation is that many of these propellants extinguish at high pressures.[1] The reason for this extinguishment is thought to be due to two conditions: (1) the position of the oxidizer particles relative to the binder surface as a

[1]The approximate upper deflagration limit is denoted by x in Fig. 2.2.

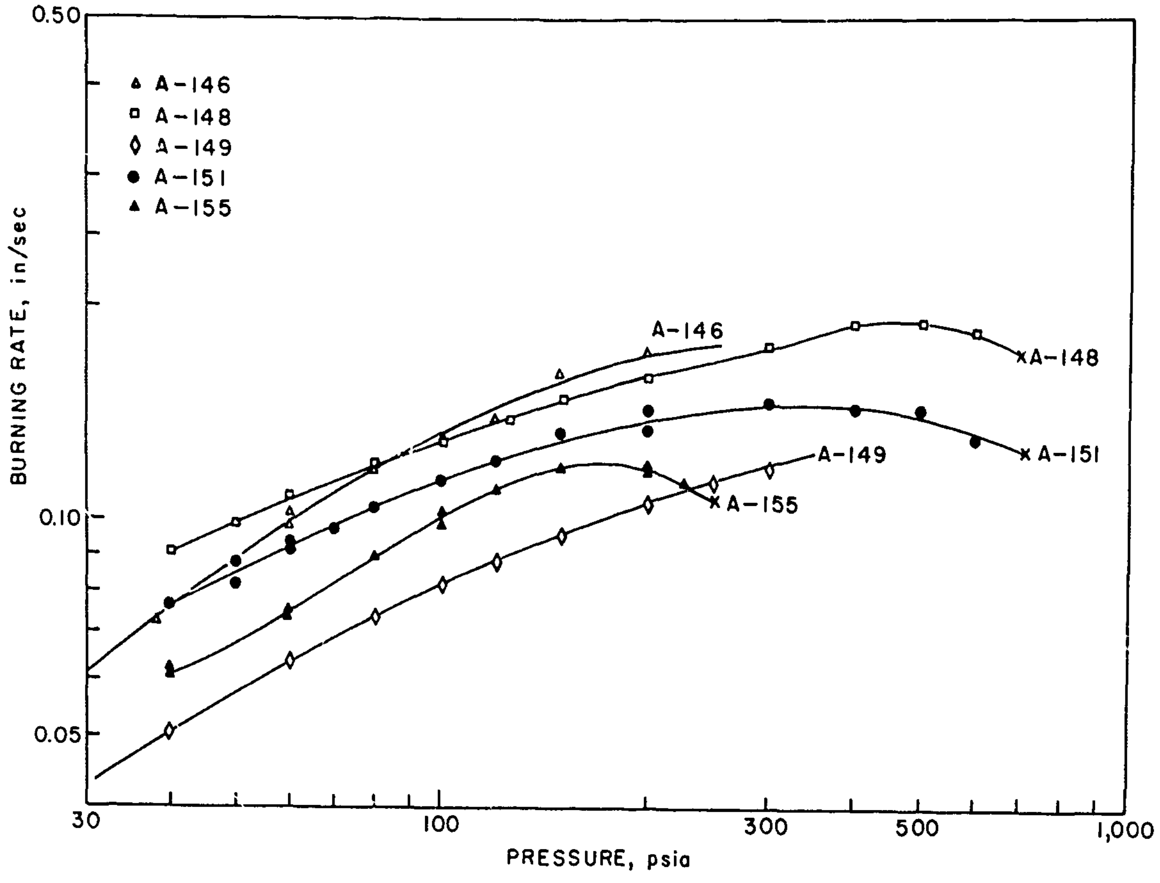

FIG. 2.2. Burning Rate Curves for Polyurethane-Ammonium Perchlorate Propellants.

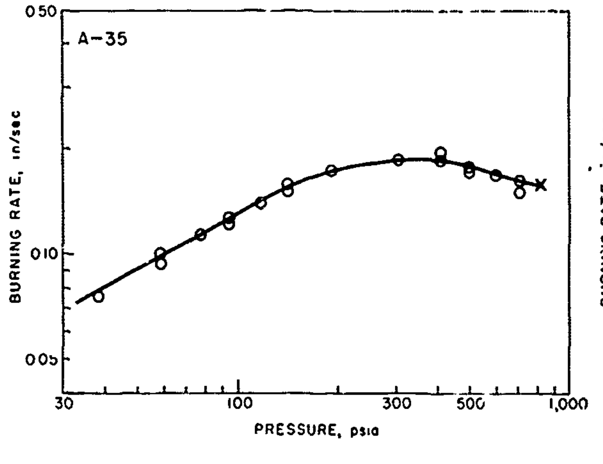

FIG. 2.3. Burning Rate Curve for Propellant A-35.

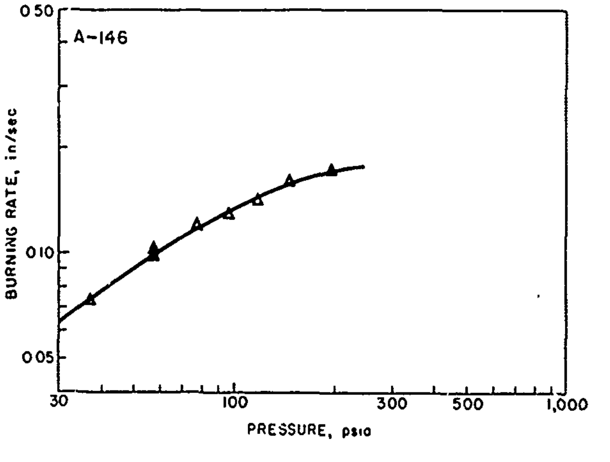

FIG. 2.4. Burning Rate Curve for Propellant A-146.

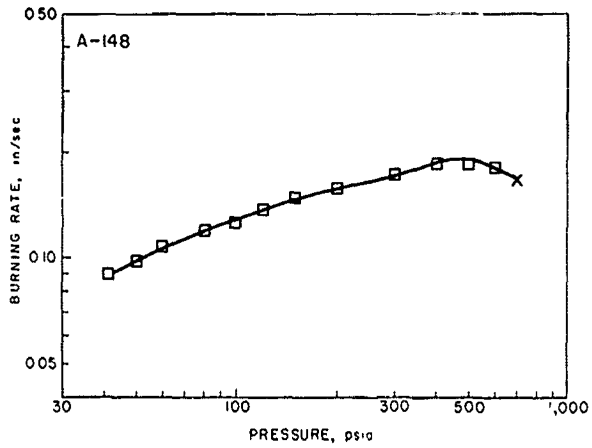

FIG. 2.5. Burning Rate Curve for Propellant A-148.

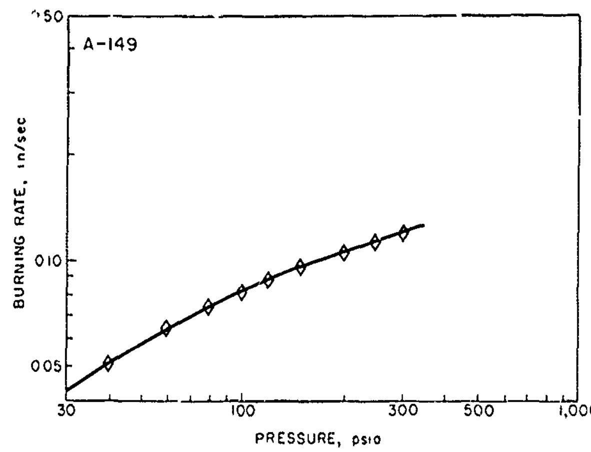

FIG. 2.6. Burning Rate Curve for Propellant A-149.

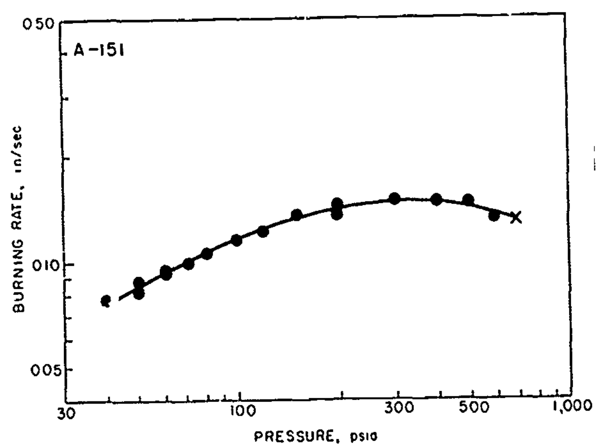

FIG. 2.7. Burning Rate Curve for Propellant A-151.

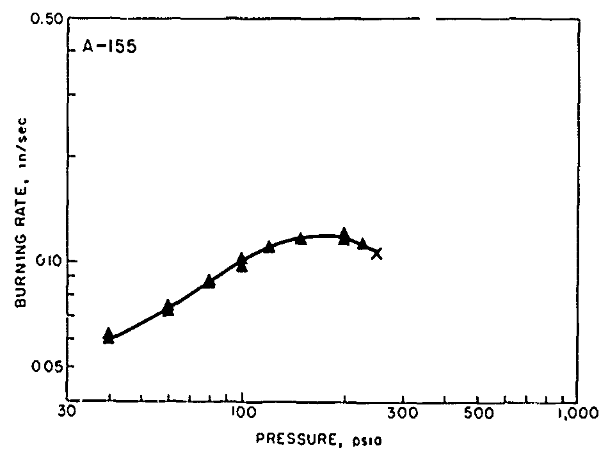

FIG. 2.8. Burning Rate Curve for Propellant A-155.

function of pressure, and (2) the meltability of the binder. It has been observed (Ref. 4) that at low pressures ($p < 600$ psia) the regression rate of the binder was higher than the oxidizer particles but at higher pressures ($p > 800$ psi) the opposite was found to be true. Therefore, an extinguishment mechanism may be formulated to account for the high pressure extinguishment of polyurethane propellants; at low pressures the oxidizer is above the binder so that the meltability of the binder has little effect but when the regression rate of binder and oxidizer are about equal, the molten binder may wet and cover the oxidizer particles. Such behavior could cause extinguishment and this hypothesis is currently being investigated using cinephotomicrography and scanning electron microscope (SEM) examination of quenched samples.

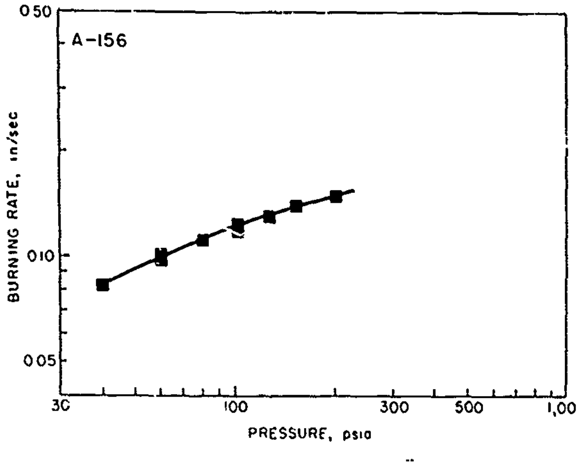

FIG. 2.9. Burning Rate Curve for Propellant A-156.

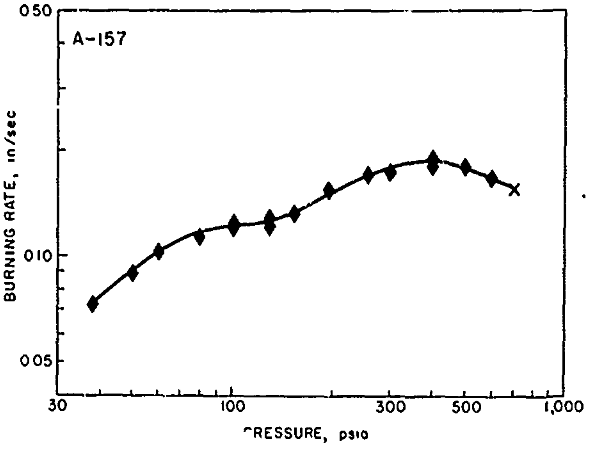

FIG. 2.10. Burning Rate Curve for Propellant A-157.

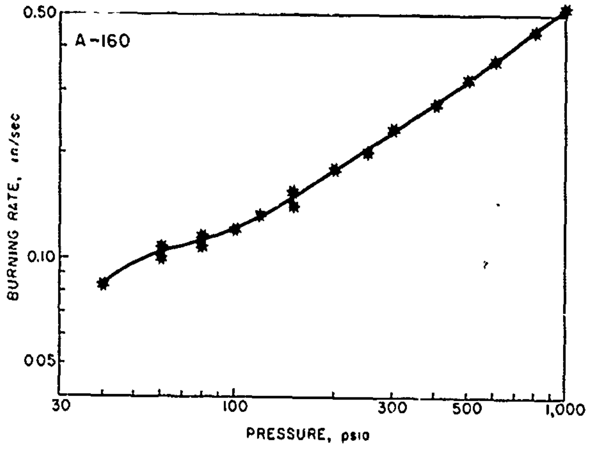

FIG. 2.11. Burning Rate Curve for Propellant A-160.

The trend of higher burning rates for propellants having smaller oxidizer particles (Ref. 5)is apparent when the curves for propellants A-146 (15- and 90-micron AP particles) and A-148 (15- and 200-micron AP particles) are compared with the A-149 (90- and 600-micron AP) and A-155 (45- and 400-micron AP) propellants. The study of quenched propellant samples using the SEM may suggest the mechanism for this well recognized observation.

The data for propellant A-160 (Fig. 2.11) show that often the plateau and mesa-burning-rate characteristics can be altered by additives as well as by AP-particle-size changes.

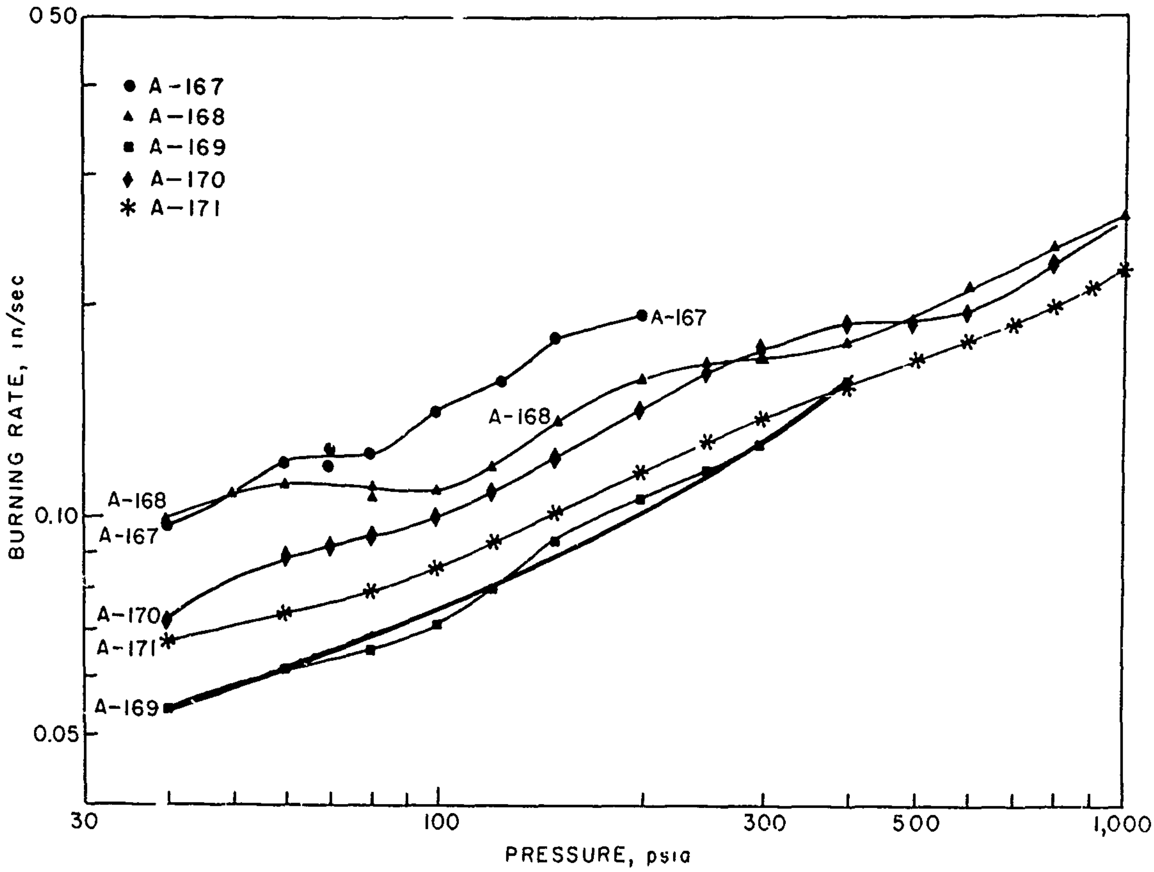

FIG. 2.12. Burning Rate Curves for Carboxy-terminated Polybutadiene-ammonium Perchlorate Propellants.

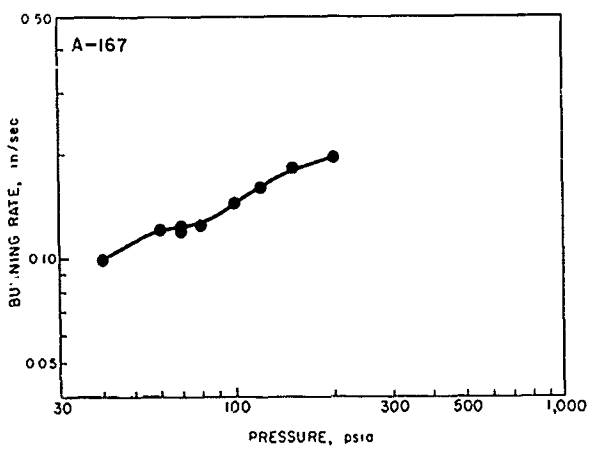

FIG. 2.13. Burning Rate Curve for Propellant A-167.

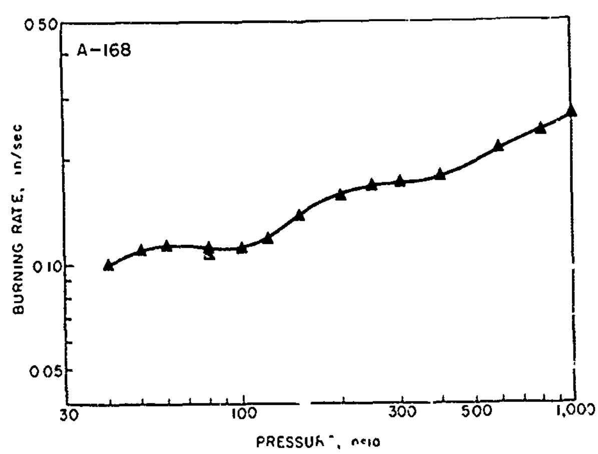

FIG. 2.14. Burning Rate Curve for Propellant A-168.

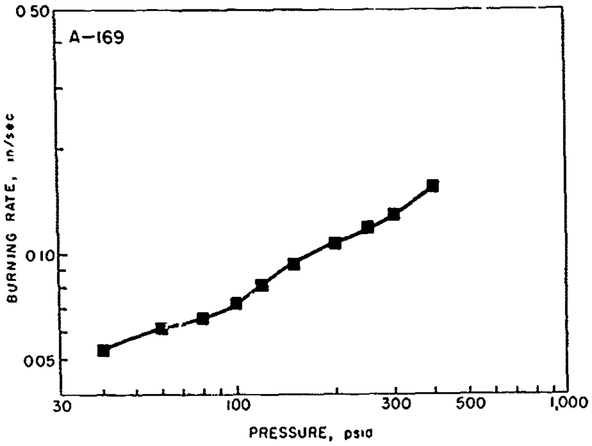

FIG. 2.15. Burning Rate Curve for Propellant A-169.

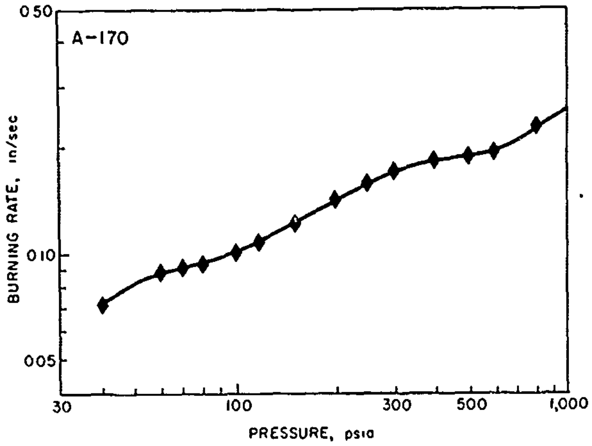

FIG. 2.16. Burning Rate Curve for Propellant A-170.

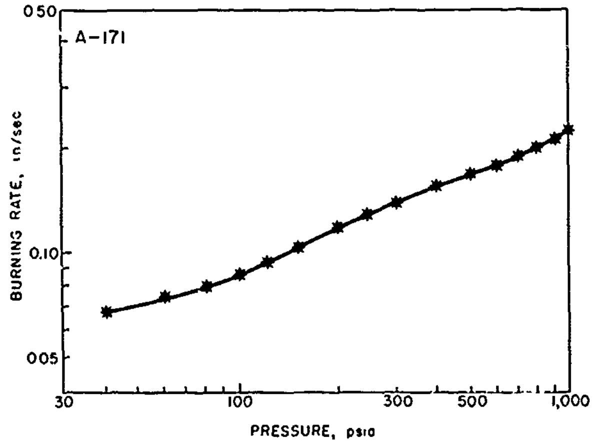

FIG. 2.17. Burning Rate Curve for Propellant A-171.

The type of binder also influences the shape of the burning-rate curve as seen when Fig. 2.2 and 2.12 are compared. The CTPB propellants do not exhibit the mesa characteristic and extinguishment behavior as did the polyurethane propellants. A simple slow heating rate test used by Steinz, et al. (Ref. 6) showed that polyurethane liquifies at low temperatures ($T > 150^{\circ}C$) whereas CTPB gasifies without melting. Preliminary results indicate that the same behavior may also occur when the binders are subjected to the high heating rates which occur during combustion. Quenched samples of CTPB propellants will also be subjected to examination using the SEM; the object will be to ascertain if the propellant burns with a dry binder surface.

2.4 COMPARISON WITH ANALYTICAL MODELS

A number of analytical models have been proposed for steady-state burning of solid propellants (Ref. 5-7, see also references cited in Ref. 6). Of these, the granular diffusion flame (GDF) model of Summerfield, et al., (Ref. 8) seems to provide the best correlation of the ammonium perchlorate propellant data. Although the model is not developed from a fundamental, analytical representation of the three dimensional details of the combustion zone (no conservation laws are used), its authors claim to have originated the correct physical-chemical model (Ref. 6) which correlates most of the experimental burning rate data. These claims have been progressively qualified by recognition that the model only applies to a certain range of propellant formulations (referred to as "normal" propellants). By such a definition of normalcy, many in-service propellants have been excluded from the class of "normal" propellants for processing characteristics such as: (1) a relatively high fuel to oxidizer ratio, (2) a coarse oxidizer particle size ($d > 250$ microns), (3) a "meltable" binder. The burning rates of propellants which have a bimodal oxidizer particle size distribution (discussed below) indicate that the GDF model also does not adequately represent the effect of oxidizer particle size distribution.

The GDF model predicts that the burning rate will be related to pressure according to the expression $p/r = a + bp^{2/3}$, where $\underline{a}$ is a function primarily of thermochemical properties of the propellant and $\underline{b}$ is primarily a function of oxidizer particle size. This expression predicts that plots of p/r vs $p^{2/3}$ will be straight lines, with a single value of the intercept $\underline{a}$ for a given chemical composition of propellant. Thus the plots of data for any series of propellants having equal amounts of identical binder, the same percent of ammonium perchlorate, and equal amounts of identical additives, should be a series of straight lines, which may have different slopes but which have the same p/r intercept. Results of the present studies are replotted in Fig. 2.18 and 2.19 as p/r vs $p^{2/3}$.

The results in Fig. 2.18 for the polyurethane propellants obviously are not in accord with the GDF model. Since the polyurethane binder is believed to melt at the burning surface, it would be classed by the authors of the GDF model as "abnormal," although it is in extensive use in service rockets. At the present time there seems to be no analytical model that correlates the behavior of these propellants.

The CTPB propellants used in this investigation conform to the currently stated definition of "normal" propellants for the GDF model, with the possible exception in one instance of an upper limit on oxidizer particle size (formulation A-169). The degree of correlation by the GDF model is much better than in the case of the polyurethane propellant, although the remaining discrepancies merit note. In particular, there are important (for the practical use of propellants) detailed deviations of the burning rate from the straight line p/r vs $p^{2/3}$ correlation, which vary according to the combinations of coarse and fine AP in the bimodal mix.

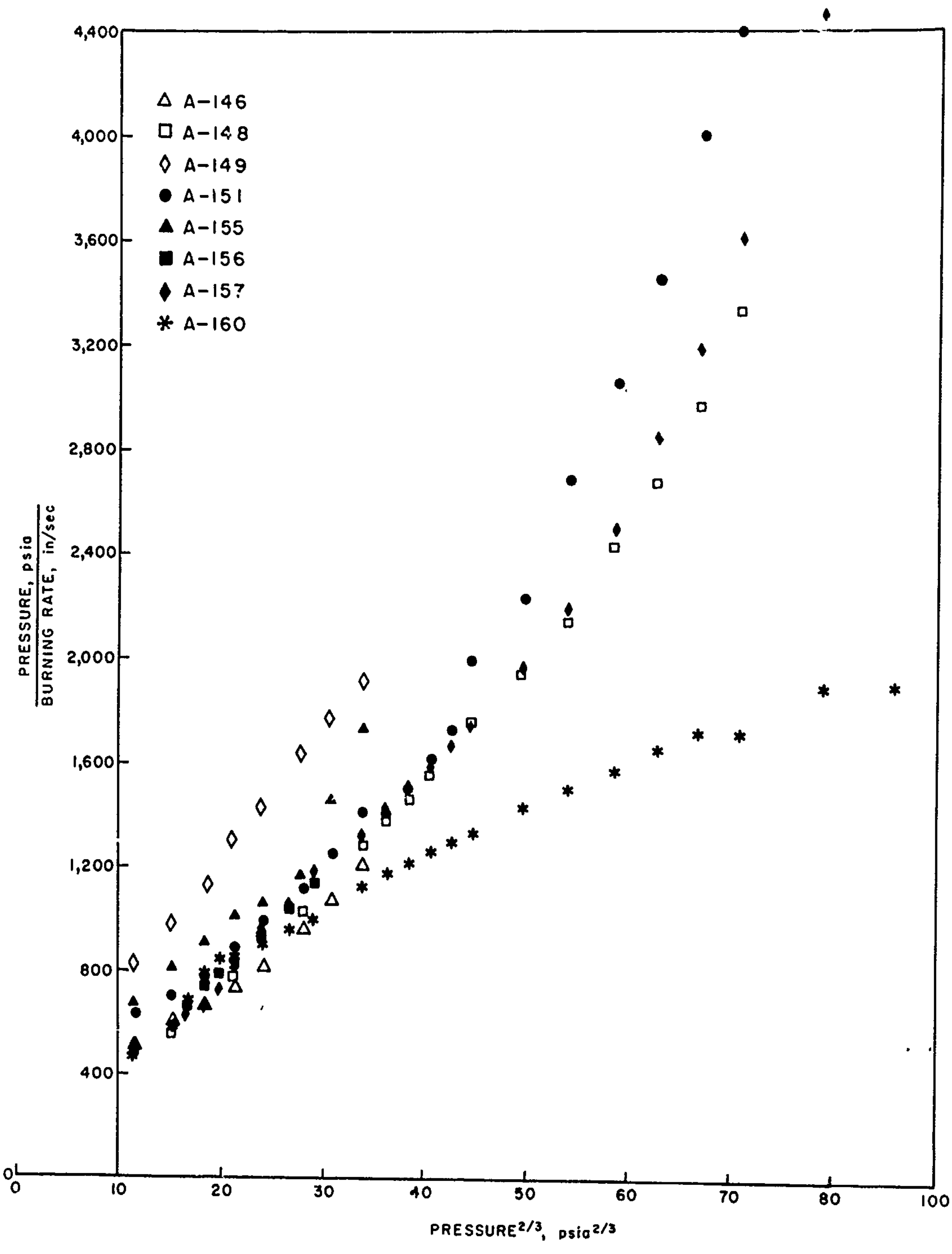

FIG. 2.18. Data from the Polyurethane-Ammonium Perchlorate Propellants Plotted in the Manner Suggested by the Granular Diffusion Flame Model Correlation.

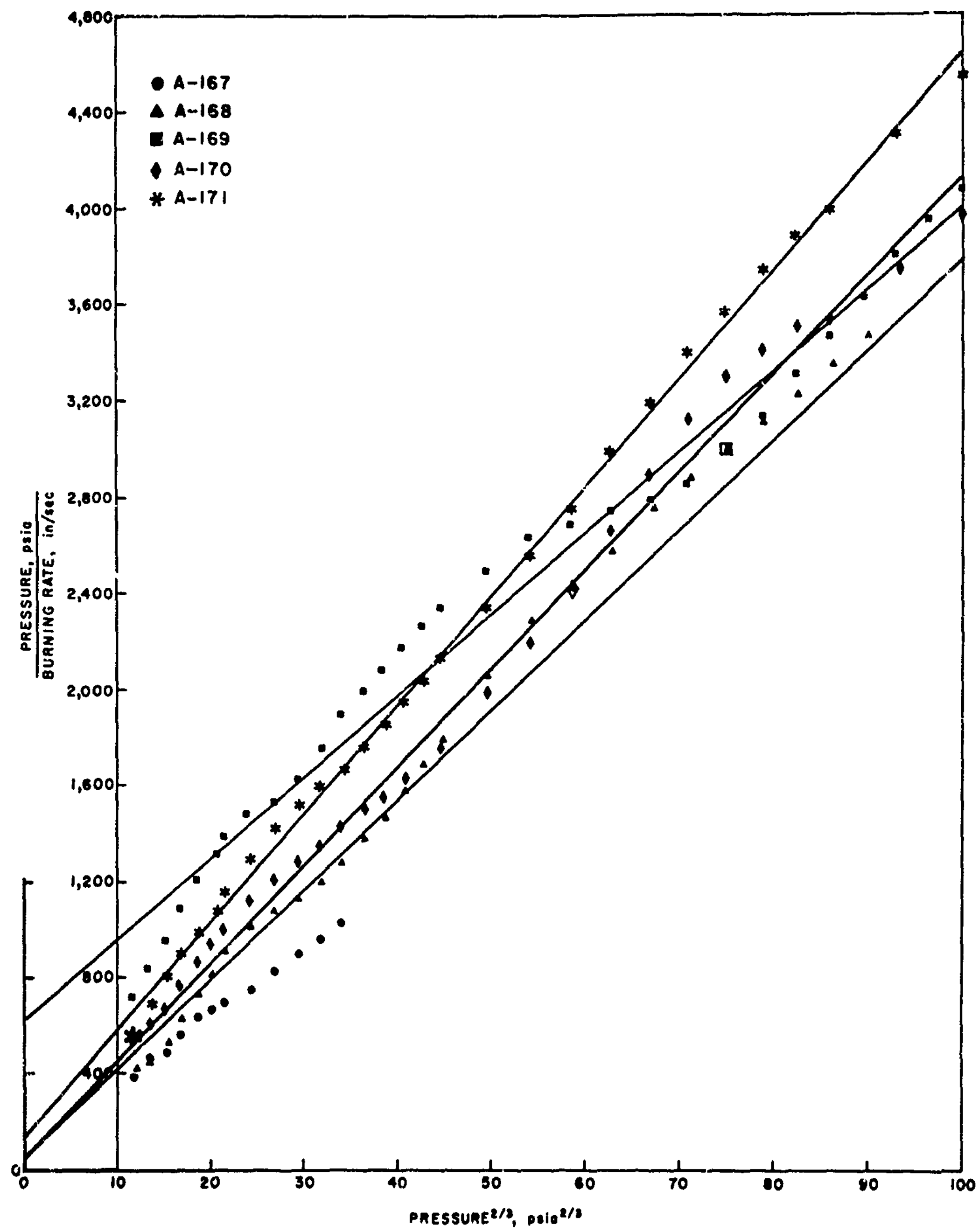

FIG. 2.19. Data from the Carboxy-Terminated Polybutadiene Propellants Plotted in the Manner Suggested by the Granular Diffusion Flame Model Correlation. The straight lines indicate a least square fit for data.

Values of a and b calculated from least squares fits to a straight line of the various sets of CTPB data are shown in the table below.

Propellant	a	b
A-168	52.8	37.6
A-169	622.1	34.0
A-170	58.8	40.8
A-171	131.6	45.2

As can be seen, there is considerable variation in the value of the intercept a as a function of particle size combinations (even when A-169 is excluded), even though a is supposed to depend only on chemical composition. The trend of the diffusion time parameter b does conform qualitatively to that predicted by the GDF model, although there is some ambiguity arising from proper definition of effective particle size relevant to this parameter.

2.5 CONCLUSIONS AND IMPLICATIONS FOR FUTURE WORK

1. Mesa burning rate curves and extinguishment at high pressures were observed with polyurethane binders, observations that may be of both practical and fundamental importance. This behavior may be due to a fluid nature of the binder at the burning surface, a point that will be explored further in future work by photographic and SEM techniques.

2. No analytical model accurately predicts the dependence of burning rate on pressure for the polyurethane-class of propellants.

3. The dependence of burning rate on pressure with the CTPB propellants was correlated roughly by the GDF model, but with some discrepancies of qualitative importance. The disagreement is related to the particle size distribution, an attribute of the propellant not embodied in existing analytical models.

4. In view of the complicated dependence of r on p observed in the present work, indiscriminate use of burning rate rules such as $r = cp^n$ or $r = a + bp^{2/3}$ is unwise. In particular, the use of $r = cp^n$ in the several perturbation models for solid propellant combustion must lead to some misrepresentation of the pressure dependence of the response function.

3. NONACOUSTIC COMBUSTION INSTABILITY

3.1 INTRODUCTION

The typical composite propellant is composed of a heterogeneous mixture of a solid oxidizer, polymeric fuel, and often a metallic additive. Because the mathematics involved in describing the combustion dynamics of such a heterogeneous mixture are quite complex, the assumptions of a one-dimensional combustion zone and a homogeneous solid are often made in order to make the problem tractable. This disregard for the heterogeneity of the propellant combustion zone is a valid assumption as long as the thermal-wave thickness is considerably larger than the individual ingredient size (i.e., oxidizer or fuel pocket size).

Since the thermal-wave thickness is often of the same order as the individual ingredient sizes for conventional composite propellants, it might be expected that the propellant heterogeneity could cause a noticeable deviation of experimental data from the one-dimensional theory. Therefore, a program was initiated to qualitatively assess what effects oxidizer particle size and binder type have on nonacoustic instability (NAI) behavior. Two series of propellants were formulated using ammonium perchlorate (AP) and either polyurethane (PU) or carboxy-terminated polybutadiene (CTPB) binder. The AP was carefully screened and the resulting 15-, 45-, 90-, 200-, 400- and 600-micron-diameter particles were mixed with the binders to produce the propellants described in Table 2.1. These propellants were fired in the L*-burner at this Center. The data for the PU-AP propellants were presented in Ref. 1 and 2.

3.2 LAYER-FREQUENCY CONCEPT

A preliminary concept, called the layer-frequency concept, was also described in Ref. 1 and 2. This layer-frequency concept pictured a propellant as layers of oxidizer particles stacked one on top of another and surrounded by binder. The characteristic time to burn through an oxidizer particle would be the diameter of the particle divided by the mean burning rate, i.e. $\tau = D/r$; this time would be repeated at a frequency of one cycle per particle within the stack. These minute pulsations, if in phase with one another over a part of the burning surface, could produce pressure oscillations having a frequency of $f = 1/\tau = r/D$.

The data presented in Ref. 1 and 2 indicated that when the thermal-wave thickness was on the order of the oxidizer particle size the one-dimensional analysis did not agree with the instability observed. Instead the data tended toward the higher frequencies as indicated by the layer-frequency concept. The concept of the layer frequency was also strengthened when two frequencies for the same run were observed as would be expected for propellants having a bimodal blend of oxidizer particle sizes. The layer-frequency computational scheme did therefore provide some insight into NAI.

3.3 RECENT EXPERIMENTAL RESULTS

The data obtained with the CTPB-AP propellants are presented in this section. Before discussing these data a few qualitative remarks comparing the oscillatory behavior of the PU-AP and the CTPB-AP propellants should be made. The CTPB-AP propellants produced more severe oscillations than did the propellants having the polyurethane binder; i.e., the amplitude of oscillations was greater for the CTPB propellants. Not only were the oscillations more severe but they were also "cleaner" and of longer duration, which made the determination of growth constants (Appendix A) less subject to errors.

From the discussions in Ref. 1 and 2 the greatest departure from one-dimensional theory would be expected at high values of burning rate (smaller thermal-wave thickness) and for large oxidizer particle sizes. This general trend with burning rate is illustrated by the data plotted in Fig. 3.1 and tabulated in Appendix A. The shaded parabolic band represents the predictions of one-dimensional theory; it is at the higher values of burning rate, r > 0.11 in/sec, that the data deviate most significantly from this band. At the lower values of burning rate the experimental data agree moderately well with the predictions of one-dimensional analysis.

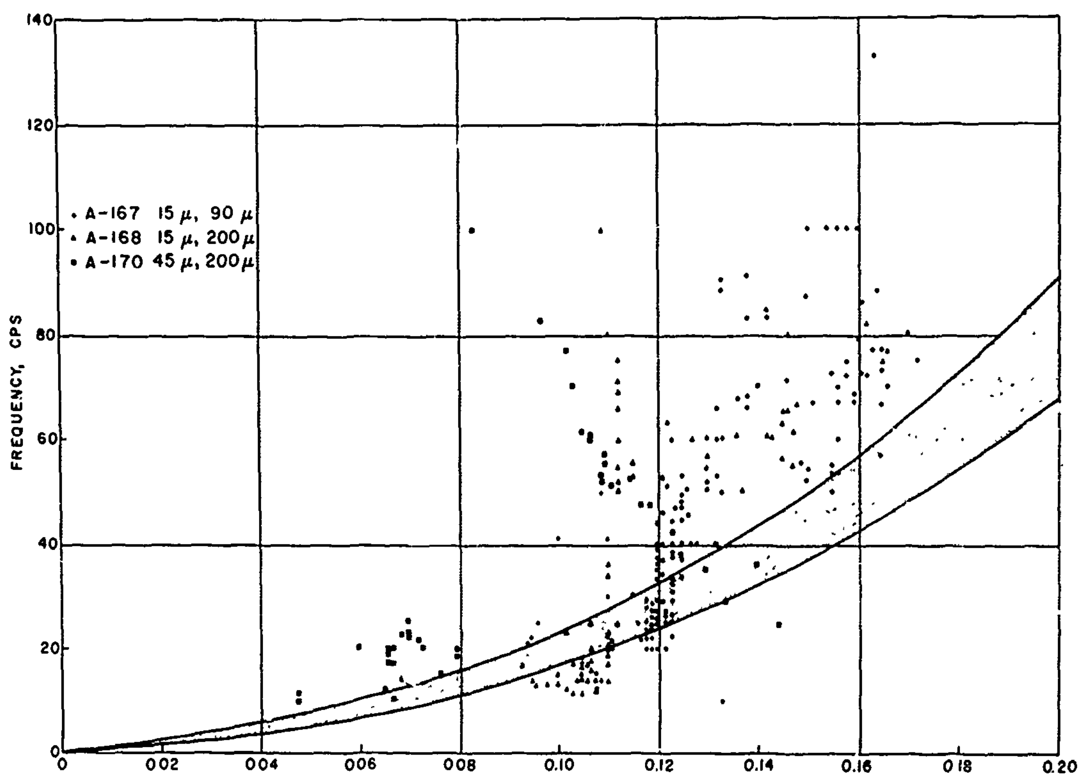

FIG. 3.1. Nonacoustic Combustion Instability Data for Three Carboxy-Terminated Polybutadiene-Ammonium Perchlorate Propellants.

Figure 3.2 presents the data for propellant A-167 which had 15- and 90-micron oxidizer particles. The most significant deviation from the one-dimensional analysis occurs for burning rates above 0.12 in/sec; the thermal-wave thickness for this rate is approximately 32 microns.

Propellant A-168 (Fig. 3.3) with 15- and 200-micron particles deviates from the parabolic band for rates above 0.11 in/sec; the corresponding thermal-wave thickness is 40 microns. Also, propellant A-170 (Fig. 3.4) with 45- and 200-micron particles also deviates from the parabolic band for rates above 0.08 in/sec with a corresponding thermal-wave thickness of 55 microns.

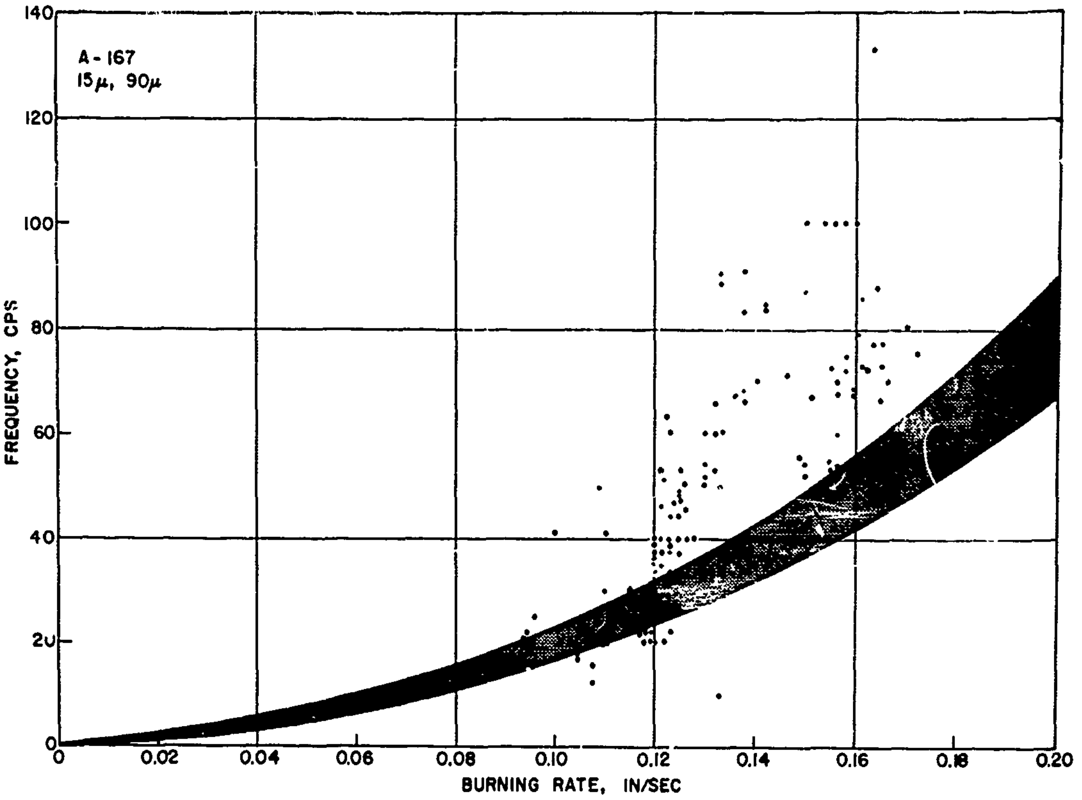

FIG. 3.2. Nonacoustic Combustion Instability Data for Propellant A-167.

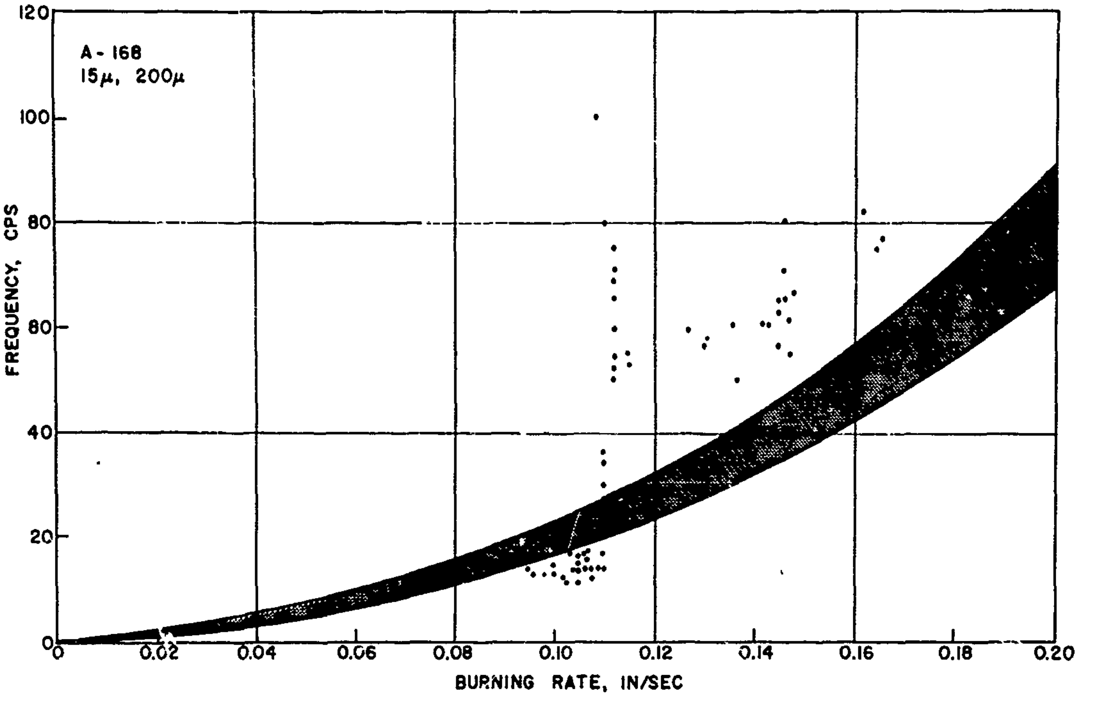

FIG. 3.3. Nonacoustic Combustion Instability Data for Propellant A-168.

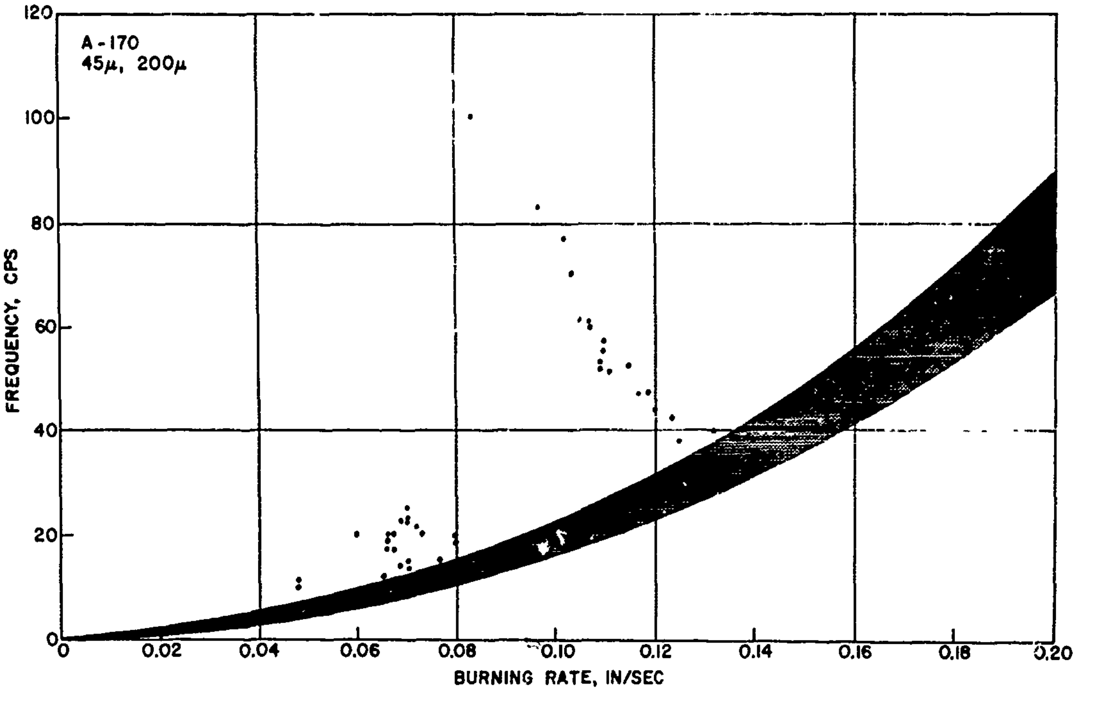

FIG. 3.4. Nonacoustic Combustion Instability Data for Propellant A-170.

3.4. SUMMARY AND IMPLICATIONS FOR FUTURE WORK

The results of this study indicate that one-dimensional analyses cannot be applied indiscriminately to combustion instability in the low-frequency regime ($f \sim 200$ cps and lower). When conditions are such that the thermal-wave thickness is approximately equal to oxidizer particle size, the physical size of the oxidizer is a contributing (and possibly a dominating) factor of combustion instability. How this interaction of the thermal wave and oxidizer affects the response function of the propellant is presently being assessed. The simple layer-frequency concept also appears to be inadequate.

Additional L* tests are being run with other CTPB-AP propellants. It is hoped that future data together with data already gathered will provide a basis for a more rigorous analysis to be made.

4. ACOUSTIC COMBUSTION INSTABILITY

In describing the transient processes involved in unstable combustion, various assumptions regarding combustion and flow behavior are made to simplify discussion and mathematical modeling. The most common assumption is that the combustion zone is thin compared to the wave length of the acoustic disturbance. A more stringent assumption is that the transit time through the combustion zone is long compared to a period of oscillation. While this latter assumption has been widely used in combustion perturbation theory, it is clearly violated at frequencies below a few hundred cycles per second. Some recent analytical and experimental studies have been directed at evaluation of the implications of this question, partly to determine how much effect to expect on calculated values of combustion response functions, and partly to determine how well our "understanding" of the combustion conforms with the actual combustion process.

In the present studies, an analytical representation of the oscillatory flow field outside the combustion zone was set up and coded for computer. The analysis assumes that each element of gas behaves isentropically in the oscillatory flow field (no diffusion). The combustion zone is characterized as an oscillatory flow source with amplitude and phase oscillations being pressure amplitude-dependent boundary parameters. The frequency dependence of these parameters would have to be determined by combustion-zone modeling or experiment, but are treated as parameters in the computer program. The program provides for calculation of the oscillatory temperature field and streak lines in the region above the combustion zone; comparison with experimentally measured streak pictures is shown in Fig. 4.1.

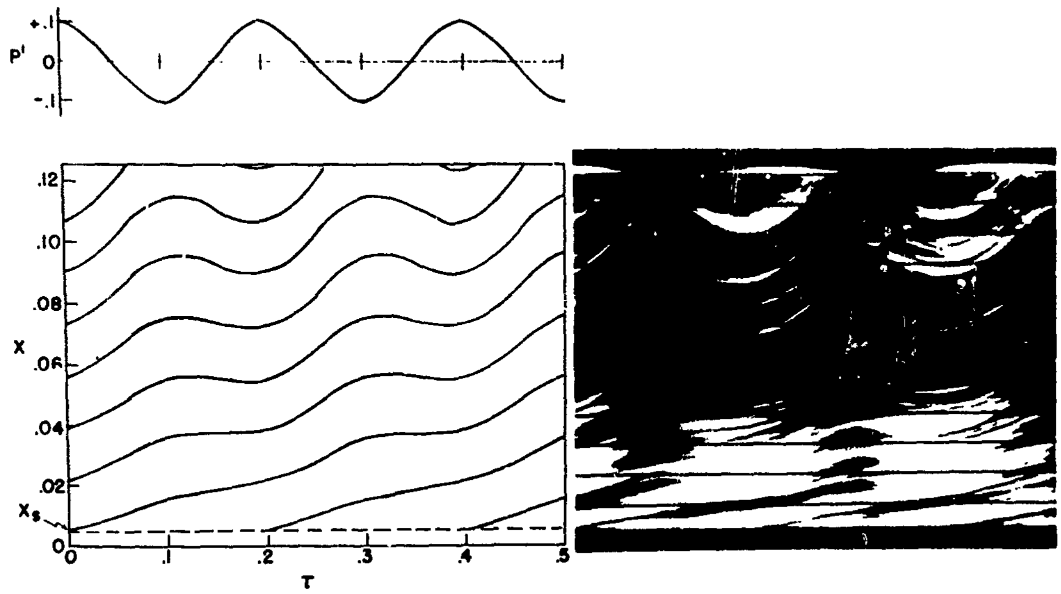

FIG. 4.1. Comparison Between Computed Trajectories and Actual Test Data. Both portions of the figure are on the same scale. Coordinates of the computed part are in dimensionless units of distance from the burning surface (x) and time (τ). Evenly spaced lines on the streak film are one inch apart on the burner and the length of the film represents 20 milliseconds. The relationship of the acoustic pressure to particle trajectories is illustrated separately in the case of the computed results, while the acoustic pressure appears as a light line on the photographic record. Computed trajectories are for particles which left the burning surface when the acoustic pressure is a maximum. All trajectories start from a reference plane, designated x_s in the figure. (From Test No. 5114 at 4.00 seconds. Mean pressure is 74 psia, acoustic pressure amplitude is 15 psi p-p, burner length 100.5 inches, frequency 125 cps. Propellant contains 25% polyurethane binder, 0.04% NaCl, remainder is 80μ spherical ammonium perchlorate.)

The equations to be solved are expressed in nondimensional variables. They are:

$$p' = \varepsilon_p \cos(n\pi x) \cos(n\pi t + \psi) \tag{4.1}$$

$$T'_s = \frac{\gamma-1}{\gamma} \varepsilon_p \varepsilon_T \cos(n\pi x_s) \cos(\psi + \beta) \tag{4.2}$$

$$T'_g = \frac{\gamma-1}{\gamma} \varepsilon_p \{\cos(n\pi x) \cos(n\pi t + \psi) - \cos(n\pi x_s) \cos\psi\} \tag{4.3}$$

where p' is the instantaneous acoustic pressure, T'_s is the fluctuation of the gas temperature at a reference plane which is a distance x_s from the propellant, T'_g is the fluctuation of the gas temperature due to acoustic pumping, x is the displacement from the propellant surface, ψ is the phase of the acoustic pressure at the time of emergence of a particle, β is the phase between pressure and reference plane temperature, ε_p is the amplitude of the pressure fluctuation, and ε_T is a measure of the isentropicity of the temperature-pressure relationship at x_s ($\varepsilon_T = 1$ if isentropic, $= 0$ if isothermal).

The gas temperature fluctuation at any point in the flow is given by

$$T' = T'_s + T'_g \tag{4.4}$$

The above equations involve a space variable "x" and a time variable "t" which are related by the following equation:

$$\frac{dx}{dt} = \overline{M} + \frac{\varepsilon_p}{\gamma} \sin(n\pi x) \sin(n\pi t + \psi) \tag{4.5}$$

where $\overline{M}$ is the dimensionless mean gas velocity. Solution of Eq. 4.5 provides the trajectory of a gas particle leaving the propellant surface and also takes acoustic flow perturbations into account.

An outline of the digital computer program used to solve the above set of equations appears in Appendix B. Eight dimensionless input parameters, derived from conditions prevailing at a particular time during an experiment, are required for a set of solutions. Output data are in the form of dimensionless parameters such as displacement of a gas element, the acoustic pressure, temperature at the reference plane, gas temperature. and total temperature as functions of time and phase of emergence of the gas element. A portion of a typical computer solution appears in Appendix C.

Comparison between computed trajectories and experimental data has been made at several test conditions in the 5.5-inch diameter T-burner. Gas motion in the burner was recorded using the special test section containing a slit window and the streak camera in an experimental arrangement that has been previously described (Ref. 2). Figure 4.1 shows a comparison between computed results and streak camera data. The two portions of the figure are on the same scale. Comparison of the computed trajectory with the experimental data indicates that the model describes gas motion in the burner with reasonable accuracy.

The next phase of this study is to determine the oscillatory temperature field and compare it with calculated fields. Ideally, the analytical aspects of this effort would be accomplished by combining the flow field analysis with a model of the combustion zone behavior, as was attempted in Ref. 10. However, preliminary results suggest that available models of the combustion zone dynamics are not realistic enough to provide argument with the experiments, and future work will involve an interlocked development of theory and diagnostic experiments designed to identify the requirements for a realistic analytical model. Temperature measurements will be made in the flow field and will be compared with temperature predicted for various models of the combustion zone to determine which seems most applicable.

Appendix A

NONACOUSTIC INSTABILITY DATA FOR A-167, A-168, AND A-170 PROPELLANTS

TABLE A-1. Data Obtained With A-168 Propellant.

Run no.	L*, in	Frequency, cps	Pressure, psia	Burning rate in/sec	Growth constant, sec^{-1}	τ_{ch}, msec	Dimensionless frequency $\frac{a_t \omega}{\bar{r}^2}$	$\omega\tau_c$	Real part of the response function
1401	42.7	14.0	50.0	0.109	−3.0	2.10	1.351	0.18442	0.99
1402	24.1	22.0	52.0	.110	...	1.18	2.089	.16357	...
1402	28.0	21.0	54.5	.111	...	1.37	1.964	.18140	...
1414	34.8	53.0	106.5	.117	...	1.71	4.396	.56901	...
1421	45.3	57.0	131.0	.128	...	2.22	3.963	.79659	...
1422	31.5	25.0	58.0	.111	...	1.55	2.306	.24295	...
1424	29.2	25.0	49.0	.108	...	1.43	2.437	.22521	...
1463	30.3	15.0	41.0	.101	12.7	1.49	1.675	.14022	1.02
1463	35.2	13.0	43.0	.104	7.3	1.73	1.387	.14117	1.01
1464	41.8	100.0	51.0	.109	...	2.05	9.569	...	...
1464	42.5	80.0	54.0	.110	13.9	2.09	7.501	...	1.03
1464	42.8	71.0	58.0	.111	11.1	2.10	6.548	.93749	1.02
1464	43.3	60.0	58.0	.111	...	2.13	5.534	.80150	...
1464	45.5	52.0	72.0	.112	...	2.23	4.728	.72992	...
1464	47.8	55.0	91.0	.114	−13.2	2.35	4.812	.81106	0.97
1464	48.2	66.0	88.0	.113	−15.8	2.37	5.893	.98142	0.96
1464	48.6	50.0	81.0	.112	−37.9	2.39	4.519	.74967	0.91
1464	51.0	17.6	35.5	.093	...	2.50	2.343	.27691	...
1465	24.4	60.0	133.0	.129	57.6	1.20	4.125	.45221	1.07
1465	37.8	50.0	143.5	.135	...	1.86	3.151	.58354	...
1465	49.7	57.1	158.5	.143	−20.9	2.44	3.180	.87620	0.95
1465	56.0	55.0	163.5	.146	...	2.75	2.946	.95020	...
1467	30.0	17.0	46.0	.106	16.9	1.47	1.721	.15734	1.02
1487	36.3	13.0	39.5	.099	...	1.78	1.510	.14558	...
1487	39.7	14.0	37.5	.096	...	1.95	1.731	.17147	...
1488	48.0	13.0	38.5	.098	...	2.36	1.556	.19251	...
1488	49.4	11.0	43.5	.104	...	2.43	1.162	.16764	...
1488	52.1	12.0	47.5	.107	0.2	2.56	1.190	.19288	1.00
1488	62.0	11.0	44.5	.105	8.8	3.04	1.141	.21040	1.03
1489	26.0	17.0	53.5	.110	...	1.28	1.598	.13636	...
1490	41.6	15.0	44.5	.105	...	2.04	1.556	.19251	...
1490	43.6	17.0	46.5	.107	...	2.14	1.709	.22866	...
1491	27.2	82.0	210.5	.165	...	1.34	3.432	.68809	...
1491	37.5	77.0	220.5	.166	...	1.84	3.183	.89081	...
1493	28.0	17.0	51.5	.110	15.6	1.37	1.620	.14685	1.02
1493	32.0	14.0	48.5	.108	...	1.57	1.372	.13821	...
1494	48.2	14.0	44.0	.105	...	2.37	1.465	.20818	...
1494	55.0	14.0	47.5	.107	13.2	2.70	1.389	.23755	1.04
1495	22.5	23.0	62.5	.112	...	1.10	2.102	.15965	...
1495	29.2	27.0	55.5	.111	...	1.43	2.513	.24323	...
1496	30.5	21.0	54.5	.111	13.4	1.50	1.964	.19760	1.02
1497	50.0	14.0	45.5	.106	3.7	2.45	1.428	.21595	1.01
1497	53.9	15.0	45.5	.106	−6.5	2.65	1.530	.24943	0.98
1497	56.2	14.0	47.5	.107	...	2.76	1.389	.24273	...
1498	13.9	23.5	41.5	.102	...	0.68	2.592	.10077	...
1498	24.7	17.4	49.5	.109	...	1.21	1.688	.13259	...
1498	31.0	20.0	49.5	.109	...	1.52	1.940	.19127	...
1500	19.6	75.0	96.5	.115	...	0.96	6.522	.45350	...
1500	23.4	69.2	100.5	.116	24.6	1.15	5.917	.49956	1.03
1500	29.1	55.5	108.5	0.118	2.8	1.43	4.552	0.49825	1.00

TABLE A-1. (Contd.).

Run no.	L*, in	Frequency, cps	Pressure, psia	Burning rate in/sec	Growth constant, sec^{-1}	τ_{ch}, msec	Dimensionless frequency $\frac{a_f \omega}{\bar{r}^2}$	$\omega\tau_c$	Real part of the response function
1500	37.7	60.0	153.0	0.140	−11.8	1.85	3.494	0.69784	0.98
1500	41.6	60.9	144.0	.135	...	2.04	3.822	.78158	...
1500	45.0	63.2	158.0	.143	−54.7	2.21	3.534	.87739	0.88
1501	22.8	80.0	160.5	.144	56.1	1.12	4.386	.56271	1.06
1501	24.6	70.6	161.5	.145	50.9	1.21	3.840	.53580	1.06
1501	26.4	66.6	165.0	.147	52.2	1.30	3.527	.54243	1.07
1501	29.9	65.6	161.5	.145	37.0	1.47	3.568	.60511	1.05
1501	33.9	60.4	153.5	.140	...	1.66	3.503	.63168	...
1501	37.9	61.5	163.5	.146	−17.1	1.86	3.294	.71908	0.97
1501	45.8	65.6	158.5	.143	...	2.25	3.654	.92690	...
1502	60.0	75.0	226.5	.166	...	2.95	3.102	...	...
1503	15.8	36.4	53.5	.110	...	0.78	3.423	.17743	...
1503	21.4	34.8	55.5	.111	...	1.05	3.239	.22975	...
1503	32.0	30.0	54.0	.110	15.7	1.57	2.813	.29616	1.02
1504	25.1	27.3	53.5	.110	...	1.23	2.567	.21140	...
1504	27.3	27.2	54.5	.111	...	1.34	2.544	.22908	...
1504	25.3	29.4	57.4	.111	...	1.24	2.717	.22929	...
1504	27.4	29.4	57.4	0.111	...	1.34	2.717	0.24834	...

TABLE A-2. Data Obtained With A-170 Propellant.

Run no.	L*, in	Frequency, cps	Pressure, psia	Burning rate in/sec	Growth constant, sec^{-1}	τ_{ch}, msec	Dimensionless frequency $\frac{a_f \omega}{\bar{r}^2}$	$\omega \tau_c$	Real part of the response function
1364	28.7	20.0	38.3	0.068	25.1	1.41	4.879	0.17708	1.04
1364	31.6	17.0	37.6	.067	15.5	1.55	4.267	.16573	1.02
1364	37.2	20.0	33.7	.062	−4.3	1.83	6.014	.22953	0.99
1369	24.3	15.0	40.7	.072	11.9	1.19	3.343	.11245	1.01
1369	30.5	15.0	44.2	.076	−0.9	1.50	2.991	.14114	1.00
1404	35.0	18.0	47.0	.079	−1.1	1.72	3.334	.19436	1.00
1404	41.5	20.0	48.0	.080	−22.0	2.04	3.618	.25606	0.96
1512	23.1	25.0	39.3	.070	7.3	1.13	5.864	.17816	1.01
1512	26.5	22.6	40.2	.071	...	1.30	5.127	.18476	...
1512	28.1	22.5	38.8	.069	...	1.38	5.381	.19505	...
1512	30.3	23.0	40.2	.071	...	1.49	5.218	.21500	...
1512	31.9	21.7	41.1	.072	...	1.57	4.770	.21356	...
1512	34.6	20.0	42.0	.073	...	1.70	4.266	.21349	...
1514	37.9	18.5	37.0	.067	6.4	1.86	4.764	.21631	1.01
1514	39.9	20.0	37.5	.067	...	1.96	5.042	.24619	...
1514	41.8	17.0	37.0	.067	...	2.05	4.377	.21922	...
1514	43.3	17.9	37.9	.068	...	2.13	4.438	.23911	...
1514	45.7	17.8	37.9	.068	−4.6	2.24	4.413	.25096	0.99
1514	50.6	18.2	37.5	.067	...	2.48	4.588	.28411	...
1515	33.6	83.0	84.9	.096	...	1.65	10.219	.86036	...
1517	37.5	16.0	37.4	.067	8.9	1.84	4.050	.18500	1.02
1517	38.8	15.8	40.2	.071	11.3	1.91	3.585	.18932	1.02
1517	43.3	15.2	40.7	.072	6.7	2.13	3.388	.20328	1.01
1517	44.6	15.6	40.7	.072	...	2.19	3.477	.21460	...
1517	48.3	14.9	39.6	.070	3.8	2.37	3.456	.22198	1.01
1517	52.0	14.8	37.4	.067	−4.9	2.55	3.746	.23743	0.99
1518	23.6	22.2	33.2	.061	19.8	1.16	6.850	.16163	1.02
1518	25.4	18.2	41.2	.072	28.8	1.25	3.987	.14262	1.04
1518	27.2	16.0	41.2	.072	15.9	1.34	3.505	.13426	1.02
1518	30.0	25.9	33.0	.061	5.4	1.47	8.076	.23971	1.01
1518	35.0	25.0	28.5	.053	−5.8	1.72	10.099	.26994	0.99
1519	59.9	15.8	37.4	.067	3.9	2.94	4.000	.29178	1.01
1519	62.2	16.0	40.7	.072	−3.2	3.05	3.566	.30707	0.99
1519	66.9	15.8	36.3	.066	−8.3	3.28	4.196	.32610	0.97
1521	49.3	21.0	41.8	.073	...	2.42	4.508	.31927	...
1521	52.2	16.2	45.7	.077	...	2.56	3.100	.20068	...
1522	22.6	29.3	41.8	.073	23.3	1.11	6.290	.20429	1.03
1522	24.4	20.0	46.3	.078	17.0	1.20	3.769	.15055	1.02
1522	27.5	19.2	46.3	.078	16.8	1.35	3.618	.16289	1.02
1522	32.1	17.0	47.4	.079	12.0	1.58	3.118	.16835	1.02
1522	35.4	17.7	47.4	.079	7.2	1.74	3.247	.19330	1.01
1522	37.7	17.7	38.5	.069	11.2	1.85	4.283	.20586	1.02
1523	27.4	16.1	42.4	.074	3.6	1.35	3.390	.13609	1.00
1523	30.4	13.2	45.2	.077	...	1.49	2.560	.12380	...
1523	36.4	13.5	47.4	.079	...	1.79	2.476	.15160	...
1524	26.0	19.0	70.3	.092	14.2	1.28	2.561	.15240	1.02
1524	28.0	20.0	66.7	.091	16.2	1.37	2.774	.17276	1.02
1524	31.2	18.0	68.5	.091	10.1	1.53	2.460	.17326	1.02
1524	32.7	18.0	66.7	.091	13.7	1.61	2.497	.18159	1.02
1524	34.7	20.0	68.5	0.091	−9.9	1.70	2.734	0.21410	0.98

TABLE A-2. (Contd.).

Run no.	L*, in	Frequency, cps	Pressure, psia	Burning rate in/sec	Growth constant, sec^{-1}	τ_{ch}, msec	Dimensionless frequency $\frac{a_f \omega}{\bar{r}^2}$	$\omega\tau_c$	Real part of the response function
1524	36.2	20.0	68.5	0.091	−8.5	1.78	2.734	0.22336	0.99
1524	41.1	16.0	61.3	.088	15.2	2.02	2.338	.20287	1.03
1524	42.1	20.0	52.3	.083	−9.8	2.07	3.316	.25976	0.98
1525	46.2	19.0	49.0	.080	...	2.27	3.361	.27081	...
1525	51.7	16.0	49.0	.080	−6.9	2.54	2.830	.25520	0.98
1525	60.9	19.0	49.0	.080	...	2.99	3.361	.35697	...
1526	43.8	15.0	44.1	.076	6.2	2.15	3.000	.20269	1.01
1526	48.0	17.0	44.1	.076	9.5	2.36	3.400	.25174	1.02
1526	49.7	12.0	48.5	.080	...	2.44	2.146	.18399	...
1526	51.1	13.0	47.5	.079	5.3	2.51	2.379	.20494	1.01
1526	53.3	15.0	45.2	.077	...	2.62	2.909	.24665	...
1526	55.7	13.0	47.4	.079	−2.3	2.73	2.385	.22339	0.99
1568	26.0	35.7	203.5	.142	...	1.28	2.021	.28635	...
1568	32.7	40.0	177.0	.130	10.1	1.61	2.696	.40352	1.02
1568	39.5	47.5	147.0	.117	...	1.94	3.973	.57883	...
1568	40.5	51.0	128.5	.110	...	1.99	4.856	.63722	...
1568	48.2	25.0	212.5	.146	...	2.37	1.344	.37175	...
1569	48.2	25.0	212.5	.146	...	2.37	1.344	.37175	...
1570	21.6	−0.0	106.5	.102	...	1.06	0.000	.00000	...
1570	24.9	68.0	108.0	.103	...	1.22	7.370	.52236	...
1570	29.0	−0.0	117.5	.106	...	1.42	0.000	.00000	...
1570	34.0	52.5	121.5	.107	...	1.67	5.236	.55068	...
1571	43.0	51.8	123.5	.108	...	2.11	5.099	.68716	...
1572	86.4	10.0	37.5	.067	...	4.24	2.521	.26655	...
1572	97.0	12.0	36.5	.066	...	4.76	3.158	.35910	...
1572	100.5	10.0	24.5	.047	...	4.93	5.188	.31005	...
1573	64.3	14.5	38.0	.068	...	3.16	3.580	.28763	...
1573	68.8	14.3	38.0	.068	...	3.38	3.531	.30352	...
1573	73.4	13.9	40.0	.071	...	3.60	3.177	.31476	...
1577	18.4	74.0	74.0	0.093	...	0.90	9.720	0.42006	...

TABLE A-3. Data Obtained With A-167 Propellant.

Run no.	L*, in	Frequency, cps	Pressure, psia	Burning rate in/sec	Growth constant, sec^{-1}	τ_{ch}, msec	Dimensionless frequency $\frac{a_l \omega}{\bar{r}^2}$	$\omega\tau_c$	Real part of the response function
1353	31.5	71.0	111.2	0.144	38.4	1.55	3.921	0.68997	1.06
1353	33.9	53.0	127.4	.155	51.0	1.66	2.535	.55429	1.08
1353	41.3	60.0	128.2	.155	−45.5	2.03	2.850	.76448	0.91
1353	49.6	50.0	98.2	.136	...	2.44	3.086	.76509	...
1354	25.6	44.0	72.6	.123	42.2	1.26	3.308	.34750	1.05
1354	26.7	33.0	71.0	.123	53.6	1.31	2.511	.27182	1.07
1354	28.4	38.0	70.2	.122	51.8	1.39	2.909	.33294	1.07
1354	29.6	33.0	66.9	.121	46.1	1.45	2.593	.30135	1.07
1354	31.5	33.0	67.7	.121	31.2	1.55	2.576	.32069	1.05
1354	34.0	31.0	66.9	.121	34.7	1.67	2.436	.32516	1.06
1354	35.0	26.0	69.3	.122	34.4	1.72	2.004	.28074	1.06
1354	41.5	32.0	64.5	.119	−5.3	2.04	2.564	.40969	0.99
1355	23.0	30.0	48.1	.109	16.9	1.13	2.897	.21287	1.02
1355	23.9	28.0	52.1	.112	34.7	1.17	2.550	.20645	1.04
1355	24.6	29.0	57.0	.115	19.6	1.21	2.493	.22009	1.02
1355	25.3	29.0	52.1	.112	21.4	1.24	2.641	.22635	1.03
1355	25.7	29.0	61.9	.118	22.9	1.26	2.377	.22993	1.03
1355	26.6	25.0	56.2	.115	14.5	1.31	2.168	.20516	1.02
1355	27.3	27.0	57.0	.115	51.4	1.34	2.321	.22740	1.07
1355	28.0	29.0	57.8	.116	17.9	1.37	2.472	.25051	1.02
1355	29.5	25.0	59.5	.117	15.4	1.45	2.095	.22752	1.02
1355	31.4	22.0	59.5	.117	45.5	1.54	1.844	.21312	1.07
1355	32.9	25.0	66.0	.120	10.5	1.62	1.978	25375	1.02
1355	34.8	25.0	59.5	.117	19.0	1.71	2.095	.26840	1.03
1355	39.0	25.0	53.8	.113	−2.3	1.91	2.228	.30079	1.00
1356	46.5	22.0	55.5	.114	6.9	2.28	1.922	.31560	1.02
1356	54.4	20.0	60.3	.117	−2.2	2.67	1.663	.33565	0.99
1362	25.5	21.0	49.7	.110	10.2	1.25	1.978	.16520	1.01
1362	32.7	20.0	49.7	.110	−1.6	1.61	1.884	.20176	1.00
1372	50.4	17.0	43.5	.104	10.6	2.47	1.787	.26433	1.03
1375	27.3	25.0	38.5	.098	9.0	1.34	2.963	.21055	1.01
1375	29.6	27.0	57.0	.115	26.5	1.45	2.321	.24656	1.04
1375	32.2	29.0	58.5	.116	30.3	1.58	2.454	.28808	1.05
1375	36.0	25.0	61.5	.118	19.6	1.77	2.056	.27765	1.03
1376	46.2	18.0	43.0	.104	17.0	2.27	1.912	.25655	1.04
1376	53.0	20.0	55.5	.114	17.0	2.60	1.748	.32702	1.04
1379	24.6	22.0	57.5	.116	...	1.21	1.881	.16696	...
1379	26.2	25.0	55.5	.114	...	1.29	2.184	.20207	...
1379	27.8	25.0	58.5	.116	...	1.36	2.116	.21441	...
1379	30.0	30.0	53.5	.113	...	1.47	2.684	.27765	...
1379	31.8	22.0	49.5	.110	...	1.56	2.079	.21583	...
1379	33.6	26.0	57.5	.116	24.8	1.65	2.223	.26951	1.04
1379	36.7	26.0	62.0	.118	...	1.80	2.129	.29438	...
1380	17.8	47.0	73.5	.124	...	0.87	3.510	.25810	...
1380	20.2	33.0	77.5	.126	...	0.99	2.392	.20565	...
1380	23.9	44.0	78.5	.126	34.7	1.17	3.166	.32442	1.04
1380	27.8	38.0	72.0	.123	27.5	1.36	2.870	.32590	1.04
1381	24.5	37.0	74.5	.124	...	1.20	2.743	.27966	...
1381	27.7	40.0	71.5	.123	38.9	1.36	3.032	.34182	1.05
1381	32.9	40.0	76.5	0.125	22.6	1.62	2.921	0.40599	1.04

TABLE A-3. (Contd.).

Run no.	L*, in	Frequency, cps	Pressure, psia	Burning rate in/sec	Growth constant, sec^{-1}	τ_{ch}, msec	Dimensionless frequency $\frac{a_f \omega}{\bar{r}^2}$	$\omega\tau_c$	Real part of the response function
1381	43.0	27.0	63.5	0.119	13.1	2.11	2.182	0.35817	1.03
1382	25.2	50.0	80.0	.127	52.0	1.24	3.558	.38872	1.06
1382	35.0	45.0	83.0	.128	38.5	1.72	3.131	.48590	1.07
1383	30.8	40.0	85.5	.129	...	1.51	2.731	.38008	...
1383	38.0	40.0	84.5	.129	...	1.87	2.752	.46893	...
1384	16.8	60.0	93.5	.134	...	0.82	3.848	.31097	...
1384	18.3	66.0	93.5	.134	37.4	0.90	4.232	.37261	1.03
1384	19.3	100.0	116.0	.147	...	0.95	5.293	.59541	...
1384	22.0	66.0	98.0	.136	...	1.08	4.080	.44795	...
1384	24.3	68.0	97.0	.135	22.0	1.19	4.239	.50977	1.03
1384	26.0	87.0	116.5	.147	...	1.28	4.584	.69784	...
1384	32.0	50.0	89.0	.131	...	1.57	3.323	.49361	...
1384	34.4	36.0	84.0	.129	...	1.69	2.486	.38205	...
1386	35.8	86.0	134.0	.159	...	1.76	3.883	.94983	...
1386	27.1	88.0	141.0	.164	...	1.33	3.744	.73572	...
1386	29.5	72.0	131.5	.157	49.7	1.45	3.322	.65526	1.07
1386	31.5	100.0	128.0	.155	21.4	1.55	4.758	.97179	1.03
1386	33.5	67.0	118.5	.149	26.2	1.64	3.468	.69244	1.04
1450	21.9	33.0	68.0	.121	...	1.08	2.570	.22296	...
1450	23.7	35.0	68.0	.121	42.4	1.16	2.726	.25590	1.05
1450	25.8	33.0	65.0	.120	22.0	1.27	2.633	.26266	1.03
1450	28.3	32.0	65.0	.120	22.3	1.39	2.553	.27938	1.03
1450	36.0	27.0	63.0	.119	29.1	1.77	2.191	.29987	1.05
1451	44.5	27.3	58.5	.116	19.0	2.18	2.311	.37479	1.04
1451	55.0	20.0	59.5	.117	14.8	2.70	1.676	.33936	1.04
1454	29.7	20.0	60.0	.117	...	1.46	1.668	.18325	...
1454	36.3	24.0	61.0	.118	22.6	1.78	1.983	.26877	1.04
1454	45.0	20.0	63.0	.119	15.8	2.21	1.623	.27765	1.04
1455	24.0	37.5	58.5	.116	...	1.18	3.174	.27765	...
1455	25.4	28.6	63.5	.119	18.9	1.25	2.311	.22411	1.02
1455	27.6	30.0	69.5	.122	34.7	1.36	2.309	.25544	1.05
1455	31.3	37.5	75.5	.125	27.0	1.54	2.759	.36211	1.04
1455	39.0	32.3	74.5	.124	11.3	1.91	2.394	.38862	1.02
1456	21.0	54.0	119.0	.149	14.0	1.03	2.783	.34984	1.01
1456	21.4	52.0	123.0	.152	...	1.05	2.586	.34330	...
1456	25.7	55.0	125.0	.153	17.0	1.26	2.687	.43607	1.02
1456	30.0	50.0	127.0	.154	...	1.47	2.400	.46276	...
1456	31.1	54.0	128.0	.155	...	1.53	2.569	.51810	...
1456	34.3	54.0	128.0	.155	...	1.68	2.569	.57141	...
1457	32.3	80.0	148.0	.169	...	1.59	3.216	.79718	...
1457	34.3	77.0	143.0	.165	...	[illegible]	3.222	.81479	...
1457	36.2	73.0	143.0	.165	...	1.78	3.055	.81526	...
1457	38.2	66.0	143.0	.165	...	1.88	2.762	.77780	...
1457	40.1	57.0	143.0	.165	...	1.97	2.385	.70515	...
1457	46.1	58.0	148.0	.169	16.1	2.26	2.331	.82488	1.04
1468	16.5	40.0	63.5	.119	23.7	0.81	3.232	.20361	1.02
1468	17.9	36.4	72.5	.123	18.3	0.88	2.739	.20135	1.02
1468	19.6	37.5	78.5	.126	23.0	0.96	2.698	.22733	1.02
1468	24.1	47.4	79.5	.127	22.2	1.18	3.385	.35198	1.03
1468	36.0	52.8	93.5	0.134	...	1.77	3.386	0.58641	...

TABLE A-3. (Contd.).

Run no.	L*, in	Frequency, cps	Pressure, psia	Burning rate in/sec	Growth constant, sec^{-1}	τ_{ch}, msec	Dimensionless frequency $\frac{a_t \omega}{\bar{r}^2}$	$\omega\tau_c$	Real part of the response function
1470	22.7	720.0	163.5	0.178	...	1.11	25.869	...	...
1470	24.8	133.0	138.5	.162	...	1.22	5.778	...	...
1470	27.8	200.0	168.5	.181	24.7	1.36	6.965	...	1.03
1470	41.0	200.0	193.5	.191	122.1	2.01	6.239	...	1.25
1471	32.6	77.7	138.5	.162	34.7	1.60	3.376	0.78073	1.06
1471	37.1	73.3	136.5	.161	...	1.82	3.239	.83805	...
1471	39.6	66.6	132.5	.158	7.8	1.95	3.046	.81446	1.02
1471	41.4	67.5	132.5	.158	−16.6	2.03	3.087	.86128	0.97
1471	43.1	67.5	128.5	.155	...	2.12	3.198	.89731	...
1471	56.0	72.5	125.5	.153	...	2.75	3.527	...	...
1472	28.4	100.0	123.5	.152	45.6	1.39	4.951	.87615	1.06
1472	33.2	100.0	131.5	.157	...	1.63	4.614	...	...
1472	38.0	100.0	133.5	.159	...	1.87	4.534	...	...
1473	31.0	67.5	98.5	.136	27.8	1.52	4.156	.64555	1.04
1473	33.1	78.6	135.5	.160	35.1	1.63	3.503	.80263	1.05
1473	37.5	70.0	105.5	.140	...	1.84	4.062	.81091	...
1473	51.0	54.5	91.5	.132	...	2.50	3.551	.85749	...
1474	18.5	88.2	94.5	.134	...	0.91	5.611	.50284	...
1474	20.3	90.9	94.5	.134	44.0	1.00	5.782	.56843	1.04
1474	21.0	83.3	101.5	.138	35.6	1.03	5.001	.54095	1.04
1474	22.1	90.9	101.5	.138	41.0	1.09	5.458	.62059	1.04
1474	23.5	84.2	106.5	.141	67.2	1.15	4.844	.61018	1.08
1474	25.1	83.3	106.5	.141	37.2	1.23	4.792	.64555	1.05
1474	35.0	53.3	83.5	.128	...	1.72	3.694	.57552	...
1480	14.0	40.0	65.5	.120	...	0.69	3.179	.17326	...
1480	21.7	53.3	68.5	.121	52.0	1.07	4.135	.35731	1.06
1480	25.5	63.2	73.5	.124	40.2	1.25	4.720	.49719	1.05
1481	22.1	28.6	56.5	.115	...	1.09	2.472	.19499	...
1481	24.5	45.5	63.5	.119	42.7	1.20	3.677	.34391	1.05
1481	28.3	51.4	73.5	.124	46.8	1.39	3.838	.44876	1.07
1481	35.0	34.0	69.5	.122	26.0	1.72	2.617	.36712	1.04
1482	38.0	20.0	48.5	.109	52.8	1.87	1.919	.23446	1.10
1482	42.8	22.2	56.5	.115	11.1	2.10	1.918	.29313	1.02
1482	47.1	27.8	59.0	.117	...	2.31	2.341	.40395	...
1482	52.0	23.5	56.5	.115	13.8	2.55	2.031	.37699	1.04
1483	29.2	22.0	37.5	.097	...	1.43	2.682	.19818	...
1483	31.0	21.0	36.5	.095	...	1.52	2.636	.20084	...
1486	37.0	75.0	131.5	.157	14.0	1.82	3.461	.85610	1.03
1486	39.0	70.0	128.5	.155	...	1.91	3.316	.84222	...
1486	41.0	72.0	138.5	.162	−25.9	2.01	3.128	.91071	0.95
1486	43.0	70.0	143.5	.166	...	2.11	2.917	0.92860	...
1486	47.0	75.0	153.5	0.172	...	2.31	2.890	...	...

Appendix B

COMPUTER PROGRAM FOR PREDICTIONS OF GAS BEHAVIOR IN T-BURNER

Following is a listing of the program and subroutines for solving the equation of motion of gas and the gas temperature equations in the T-burner. The computations are executed on an RCA 1108 computer.

```
      DIMENSION A(1),DX(1),N(1),Y(1200,2),YB(2),ES(2),EB(2),I2(7),
     1MESS(13)
      COMMON PHI(50),V(7),XM,TPHI,EPG
  100 FORMAT(13A6)
 1001 FORMAT(1H+13A6)
  101 FORMAT(8I4)
 1011 FORMAT(1H0'JER='I2,5X'ND='I4,5X'NNN='I2)
  102 FORMAT(3E12.4,3I4)
  103 FORMAT(I2)
 1031 FORMAT(E12.4)
  104 FORMAT(15F4.3)
  105 FORMAT(1H05X'NS2,M,NH2='3I2,5X'A(1),YB(1)='2F4.1,5X'ET.,ES(1),ES(2
     1),ER(1),EB(2),='5E12.4)
 1051 FORMAT(1H05X'I1,I2(I),I=1,7='8I4)
  106 FORMAT(1H05X'NPHI='I2)
  107 FORMAT(1H05X'THE PHI(K) ARE'18(2X,F4.2)/20(2X,F4.2))
 1071 FORMAT(1H1'EPP='E9.4,4X'MBAR='E9.4,4X'EPT='E9.4,4X'BETA='E9.4,4X'X
     1S='E9.4,4X'GAMMA='F8.2,4X'N='F8.2)
10711 FORMAT(1H0'EPP='E9.4,4X'MBAR='E9.4,4X'EPT='E9.4,4X'BETA='E9.4,4X'X
     1S='E9.4,4X'GAMMA='F8.2,4X'N='F8.2)
 1072 FORMAT(1H0'DX,HS,XM,N(1),NRC,NLIM='3E12.4,3I4/)
  108 FORMAT(1H09X'TAU',15X'DISPL',12X'PRESS',12X'SURF T', 9X'GAS T',
     113X'TOTAL T',10X'PHI='F6.3/)
  109 FORMAT(1H 6(5X,E12.5))
  110 FORMAT(1H1)
  200 FORMAT(1H I2,3X'REDUCTIONS IN STEP SIZE ERROR BOUND EXCEEDED')
  201 FORMAT(1H 'CURSES, ND CONTROL FAILED,NNN='I2)
```

```
  202 FORMAT(1H 'CONVERGENCE WITH NNN = 'I2)
      DATA ERB/1.E-4/
      DATA PI/0202622077325/
      DATA TPI/0203622077325/
      DATA NS2,M,A(1),ETA,YB(1),ES(1),ES(2),EB(1),EB(2),NH /2,1,0.,5.E-7
     1,0.,1.E-7,1.E-7,1.E-6,1.E-6,5/
      DEFINE G(A,B,C) = COS(V(7)*PI*A)*COS(V(7)*PI*B+C)
      TAU0=0.
    1 READ (5,100,END=999)MESS
      READ (5,101) I1,(I2(I),I=1,7)
      IF (I1.EQ.0) GO TO 2
      READ (5,102) DX(1),HS,XM,N(1),NRC,NLIM
      NRC1=NRC+1
    2 DO 3 I=1,7
      IF (I2(I).EQ.1) READ(5,1031) V(I)
    3 CONTINUE
      FGAM=(V(6)-1.)/V(6)
      FGAM1=FGAM*V(1)
      EPO=V(1)/V(6)
      YB(2)=V(5)
      XS=V(5)
      BETA=TPI*V(4)
      READ (5,103) NPHI
      READ (5,104) (PHI(K),K=1,NPHI)
      WRITE (6,110)
      WRITE (6,1001) MESS
      WRITE (6,101) I1,I2
      WRITE (6,106) NPHI
      WRITE (6,107) (PHI(K),K=1,NPHI)
      GO TO(20,30),NRC1
C     START OF TIME HISTORY
   20 HST=HS
      AT1=A(1)
      DXT1=DX(1)
      NT1=N(1)
```

```
      YBT1=YB(1)
      YBT2=YB(2)
      WRITE(6,10711)V
      WRITE(6,1072) DX(1),HS,XM,N(1),NRC,NLIM
      DO 50 K=1,NPHI
      TPHI=TPI*PHI(K)
      AA=TPHI+BETA
      NNN=0
      WRITE(6,108) PHI(K)
   31 CALL USBGRK(NS2,M,A,DX,N,Y,ETA,YB,HS,ES,EP,NH,ND,JER)
      TX=Y(ND,2)
      TT=Y(ND,1)
      PP=V(1)*G(TX,TT,TPHI)
      ZT = 0.
      TSP = FGAM1*V(3)*G(XS,ZT,AA)
      TGP=FGAM*PP-FGAM1*G(XS,TAU0,TPHI)
      TTOT=TSP+TGP
      WRITE(6,109) Y(ND,1),Y(ND,2),PP,TSP,TGP,TTOT
      NNN=NNN+1
      WRITE(6,1011)JER,ND,NNN
      IF(NNN.GE.NLIM) GO TO 300
      YER=(Y(ND,2)-XM)/XM
      IF(YER.GT.0.) GO TO 301
      IF((ABS(YER)-ERB).LT..00000001) GO TO 302
      HS=HS/10.
      A(1)=Y(ND,1)
      DX(1)=DX(1)/10.
      N(1)=11
      YB(1)=Y(ND,1)
      YB(2)=Y(ND,2)
      GO TO 31
  300 WRITE(6,200)NLIM
      GO TO 501
  301 WRITE(6,201)NNN
      GO TO 501
```

```
302 WRITE(6,202)NNN
501 HS=HST
    A(1)=AT1
    DX(1)=DXT1
    N(1)=NT1
    YB(1)=YBT1
    YB(2)=YBT2
 50 CONTINUE
    GO TO 1
C   END OF TIME HISTORY
C   START OF TRAJECTORY
 30 DO 5 K=1,NPHI
    TPHI=TPI*PHI(K)
    AA=TPHI+BETA
    CALL USBGRK(NS2,M,A,DX,N,Y,ETA,YB,HS,ES,EB,NH,ND,JER)
    WRITE(6,1071) V
    WRITE(6,1072) DX(1),HS,XM,N(1),NRC
    WRITE (6,108) PHI(K)
    DO 4 I=1,ND
    TX=Y(I,2)
    TT=Y(I,1)
    PP=V(1)*G(TX,TT,TPHI)
    ZT = 0.
    TSP = FGAM1*V(3)*G(XS,ZT,AA)
    TGP=FGAM*PP-FGAM1*G(XS,TAU0,TPHI)
    TTOT=TSP+TGP
    WRITE (6,109) Y(I,1),Y(I,2),PP,TSP,TGP,TTOT
  4 CONTINUE
    WRITE(6,1011) JER,NL
  5 CONTINUE
    GO TO 1
C   END OF TRAJECTORY
999 STOP
    END
```

```
      SUBROUTINE DIFFEQ(U,W,FW)
      DIMENSION W(2),FW(2)
       COMMON PHI(50),V(7),XM,TPHI,EPG
      DATA PI/0202622077325/
      DATA TPI/0203622077325/
      DOUBLE PRECISION U
      FW(1)=1.
      TV1=PI*V(7)*W(2)
      TV2=PI*V(7)*W(1)+TPHI
      FW(2)=V(2)+EPG*SIN(TV1)*SIN(TV2)
      RETURN
      END


      SUBROUTINE CRITER(X,Y,J)
      COMMON PHI(50),V(7),XM,TPHI,EPG
      DIMENSION Y(2)
      DOUBLE PRECISION X
      IF((XM-Y(2)).LT..00000001) J=2
      RETURN
      END


      SUBROUTINE USBGRK(NS2,M, A, DX, N, Y, ETA, YB, HS, ES, EB, NH2,
     1      ND , JER )
      DIMENSION A(8),DX(8),N(8),Y(1200,2),YB(13),ES(13),EB(13),XX(13)
      DOUBLE PRECISION  X
      COMMON /BGRKCO/ NS, NH, MM,  IFST  , ESL(13), EBL (13)
      NS =   NS2
      NH =  NH2
      JER = 1
      DO 16 J = 1, NS
```

```
16   Y(1, J) = YB(J)
     NT=0
     DO 2 J= 1, M
02   NT = NT + N(J)
     I = 2
     DO 17 J = 1, NS
17   XX(J) = YB(J)
     H = HS
     K = 1
     JB = 1
     NL = 1
     IFST =  1
     DO 9 NU = 1, M
     NL = N(NU) - K
     K=.
     X = A(NU)
     IF (NU-1) 24, 14, 13
24   JER = 7
     GO TO 40
13   DELTA =        AMAX1 (1. , ABS (X))  * ETA
     V = ABS (X-XP)
     IF ( V   - DELTA) 14, 15, 15
15   JER = 2
     GO TO 40
14   DO 9 J = 1, NL
03   H =AMIN1 (H, DX(NU))
     V=J
     XP = A(NU) + V* DX(NU)
     DO 21 L = 1, NS
     ESL(L) = ES(L) *AMAX1 (ABS(XX(L)),1.E-1)
 21  EBL(L) = EB(L) *AMAX1 (ABS(XX(L)),1.E-1)
4    CALL  BGRUKT ( H , X , XX)
     IF(MM-NH) 5, 5, 11
11   JER = 3
     GO TO 40
```

```
5    CALL CRITER (X, XX, JQ)
     GO TO (19, 20) , JQ
20   JER = 4
     GO TO 40
19   IF ( (X + H) - XP) 4, 4, 30
30   HP = XP - X
     IF ( HP -  ABS (XP) * 1.49011612E-8)  36, 36, 34
34   CALL  BGRUKT ( HP , X , XX)
     IF ( MM - NH) 32, 32, 31
31   JER = 3
     GO TO 40
32   CALL CRITER ( X, XX, JQ)
     GO TO ( 30, 20) , JQ
36   DO 18 L = 1, NS
18   Y(I, L) = XX(L)
     I = I + 1
09   CONTINUE
     IF (I -NT -1) 25, 10, 25
25   JER = 6
     RETURN
10   ND  =   NT
     RETURN
40   ND = I - 1
     RETURN
     END


     SUBROUTINE  BGRUKT ( STEP, T, X)
     DIMENSION  X (13), XW(13), FX(13), FX1(13), VK(13), VM(13), XT(13)
    1 , DX(13), SFX (13),   FCT (2)
     COMMON /BGRKCO/ NS, NH, MM,  IFST  , ESL(13), EBL (13)
C    DIFFEQ (T,X,FX)  SUPPLIED BY USER.
     DOUBLE PRECISION  T, TW, TT
     DATA FCT(1), FCT(2)/4.,1./
     MM =  0
```

```
      HH =  STEP * 0.5
      GO TO  (21, 22) ,  IFST
21    IFST =  2
      CALL  DIFFEQ (T, X, FX1)
      GO TO   1
22    DO   23   I = 1,  NS
23    FX1 (I) =  FX (I)
 1    HW =  HH
      HH =  HW * 0.5
      TW =  T
      DO  2   J = 1,  NS
      XW (J)  =  X (J)
      DX (J) =  0.
      SFX (J) =  FX1 (J)
      FX (J) =  FX1 (J)
 2    CONTINUE
      DO  8  J =  1, 2
      DO  3  I =  1, NS
      VK (I) =  FX (I) * HH
      VM (I) =  VK (I)
 3    XT (I) = XW (I) + VK (I)
      TT =  TW + HH
      CALL  DIFFEQ ( TT, XT, FX)
      DO  4  I =  1, NS
      VK (I) =  FX (I) * HW
      VM (I) =  VM (I) +  VK (I)
 4    XT (I) =  XW (I) +  VK (I) * 0.5
      CALL  DIFFEQ (TT, XT, FX)
      DO  5  I = 1, NS
      VK (I) =  FX (I) * HW
      VM (I) =  VM (I) +  VK (I)
 5    XT (I) =  XW (I) +  VK (I)
      TW =  TW + HW
      CALL  DIFFEQ ( TW, XT, FX)
      DO  6   I =  1, NS
      VK (I) =  0.333333334 * ( VM (I) +  FX (I) * HH)
```

```
      DX (I) =  DX (I) +  VK (I)
    6 XW (I) =  XW (I) +  VK (I)
      CALL  DIFFEQ ( TW, XW, FX)
      DO 7   I = 1, NS
    7 SFX (I) =  SFX (I) +  FX (I) * FCT (J)
    8 CONTINUE
      A =  HW / 3.
      DO  9  I = 1,  NS
    9 DX (I) =  ABS ( DX (I) -  SFX (I) *A )
      DO  10   I = 1,  NS
      IF ( DX (I) .GT.  EBL(I) )   GO TO 11
   10 CONTINUE
      GO TO  12
   11 MM =  MM + 1
      IF ( MM .LE. NH)  GO TO  1
   12 STEP =  HW * 2.
      DO  13  I = 1,  NS
   13 X (I) =  XW (I)
      T =  TW
      DO  14  I = 1,  NS
      IF ( DX (I) .GT. ESL(I) )  RETURN
   14 CONTINUE
      STEP =  STEP * 2.
      RETURN
      END

     UNIVAC 1108 FORTRAN V COMPILATION.     0 *DIAGNOSTIC* MESSAGE(S)
```

Appendix C

SAMPLE OF TYPICAL COMPUTER OUTPUT

A portion of typical computer output data from the particle trajectory, gas temperature program appears below. Parameter values are identical to those in Fig. 4.1. The output data presented here were calculated for a gas particle which left the reference plane at an acoustic pressure maximum (ψ=0). The reference plane temperature, normally printed in a column with the other data, has been omitted since T_s has a fixed value for each value of ψ. In this case, T_s = 0.020397.

TAU	DISPL	PRESS	GAS T	TOTAL T
.00000	.50000-02	.10199+00	.00000	.20397-01
.25000-00	.74601-02	.72105-01	-.59765-02	.14421-01
.50000-00	.10277-01	.76965-08	-.20397-01	.13970-08
.75000-00	.13254-01	-.72062-01	-.34810-01	-.14412-01
.10000+01	.15896-01	-.10187+00	-.40772-01	-.20375-01
.12500+01	.17787-01	-.72012-01	-.34800-01	-.14402-01
.15000+01	.19024-01	-.53410-07	-.20397-01	-.10477-07
.17500+01	.20199-01	.71980-01	-.60015-02	.14396-01
.20000+01	.22006-01	.10176+00	-.46216-04	.20351-01
.22500+01	.24877-01	.71905-01	-.60165-02	.14381-01
.25000+01	.28727-01	.11707-06	-.20397-01	.23283-07
.27500+01	.32797-01	-.71742-01	-.34746-01	-.14348-01
.30000+01	.35910-01	-.10135+00	-.40668-01	-.20270-01
.32500+01	.37330-01	-.71630-01	-.34723-01	-.14326-01
.35000+01	.37476-01	-.27090-06	-.20398-01	-.54017-07
.37500+01	.37621-01	.71622-01	-.60732-02	.14324-01
.40000+01	.39018-01	.10123+00	-.15055-03	.20247-01
.42500+01	.42298-01	.71489-01	-.60996-02	.14298-01
.45000+01	.47176-01	.44138-06	-.20397-01	.88243-07
.47500+01	.52333-01	-.71152-01	-.34628-01	-.14230-01
.50000+01	.55914-01	-.10043+00	-.40484-01	-.20086-01
.52500+01	.56867-01	-.70977-01	-.34593-01	-.14195-01
.55000+01	.55929-01	-.75388-06	-.20398-01	-.15064-06

TAU	DISPL	PRESS	GAS T	TOTAL T
.57500+01	.55050-01	.71048-01	-.61878-02	.14210-01
.60000+01	.56040-01	.10042+00	-.31282-03	.20085-01
.62500+01	.59727-01	.70860-01	-.62256-02	.14172-01
.65000+01	.65624-01	.95496-06	-.20397-01	.19092-06
.67500+01	.71857-01	-.70294-01	-.34456-01	-.14059-01
.70000+01	.75901-01	-.99114-01	-.40220-01	-.19823-01
.72500+01	.76392-01	-.70059-01	-.34409-01	-.14012-01
.75000+01	.74382-01	-.12480-05	-.20398-01	-.24959-06
.77500+01	.72489-01	.70262-01	-.63451-02	.14052-01
.80000+01	.73076-01	.99324-01	-.53271-03	.19865-01
.82500+01	.77165-01	.70017-01	-.63941-02	.14003-01
.85000+01	.84071-01	.15584-05	-.20397-01	.31153-06
.87500+01	.91366-01	-.69173-01	-.34232-01	-.13835-01
.90000+01	.95865-01	-.97409-01	-.39879-01	-.19482-01
.92500+01	.95902-01	-.68877-01	-.34173-01	-.13775-01
.95000+01	.92837-01	-.21433-05	-.20398-01	-.42864-06
.97500+01	.89942-01	.69263-01	-.65449-02	.13853-01
.10000+02	.99130-01	.97938-01	-.80982-03	.19588-01
.10250+02	.94617-01	.68964-01	-.66048-02	.13793-01
.10500+02	.10252+00	.25756-05	-.20397-01	.51502-06
.10750+02	.11086+00	-.67793-01	-.33956-01	-.13559-01
.11000+02	.11580+00	-.95324-01	-.39462-01	-.19065-01
.11250+02	.11539+00	-.67439-01	-.33885-01	-.13488-01
.11500+02	.11129+00	-.31138-05	-.20398-01	-.62259-06
.11750+02	.10741+00	.68055-01	-.67865-02	.13611-01
.12000+02	.10721+00	.96269-01	-.11436-02	.19254-01
.12250+02	.11209+00	.67702-01	-.68571-02	.13540-01
.12500+02	.12096+00	.34987-05	-.20397-01	.69966-06
.12750+02	.13032-00	-.66161-01	-.33630-01	-.13232-01
.13000+02	.13571-00	-.92870-01	-.38971-01	-.18574-01
.13250+02	.13486-00	-.65750-01	-.33548-01	-.13150-01
.13500+02	.12975-00	-.40088-05	-.20398-01	-.80164-06
.13750+02	.12490+00	.66640-01	-.70694-02	.13328-01
.14000+02	.12431+00	.94320-01	-.15335-02	.18864-01

TAU	DISPL	PRESS	GAS T	TOTAL T
.14250+02	.12957-00	.66234-01	-.71506-02	.13247-01
.14500+02	.13941-00	.43648-05	-.20397-01	.87288-06
.14750+02	.14976-00	-.64285-01	-.33254-01	-.12857-01
.15000+02	.15557-00	-.90059-01	-.38409-01	-.18012-01
.15250+02	.15431-00	-.63818-01	-.33161-01	-.12764-01
.15500+02	.14820-00	-.48854-05	-.20398-01	-.97696-06
.15750+02	.14242-00	.65022-01	-.73931-02	.13004-01
.16000+02	.14144-00	.92094-01	-.19786-02	.18419-01
.16250+02	.14709-00	.64565-01	-.74846-02	.12913-01
.16500+02	.15785-00	.54212-05	-.20396-01	.10841-05
.16750+02	.16917-00	-.62172-01	-.32832-01	-.12434-01
.17000+02	.17539-00	-.86904-01	-.37778-01	-.17381-01
.17250+02	.17372-00	-.61652-01	-.32728-01	-.12330-01
.17500+02	.16666-00	-.63622-05	-.20399-01	-.12724-05
.17750+02	.15995-00	.63204-01	-.77567-02	.12641-01
.18000+02	.15861-00	.89596-01	-.24782-02	.17919-01
.18250+02	.16462-00	.62697-01	-.78580-02	.12539-01
.18500+02	.17630-00	.70472-05	-.20396-01	.14093-05
.18750+02	.18855-00	-.59832-01	-.32364-01	-.11966-01
.19000+02	.19516-00	-.83422-01	-.37082-01	-.16684-01
.19250+02	.19310-00	-.59261-01	-.32250-01	-.11852-01
.19500+02	.18512-00	-.79526-05	-.20399-01	-.15905-05
.19750+02	.17752-00	.61190-01	-.81594-02	.12238-01
.20000+02	.17582-00	.86831-01	-.30312-02	.17366-01
.20250+02	.18219-00	.60636-01	-.82703-02	.12127-01
.20500+02	.19474-00	.85601-05	-.20396-01	.17120-05

REFERENCES

1. U. S. Naval Ordnance Test Station. Combustion of Solid Propellants and Low Frequency Combustion Instability, by Aerothermochemistry Division. China Lake, Calif., NOTS, June 1967. (NOTS TP 4244).

2. Naval Weapons Center. Combustion of Solid Propellants and Low Frequency Combustion Instability Progress Report, 1 April-30 September 1967, by Aerothermochemistry Division. China Lake, Calif., NWC, April 1968. (NWC TP 4478).

3. ------. Decomposition and Deflagration of Ammonium Perchlorate by T. L. Boggs and K. J. Kraeutle. China Lake, Calif., NWC, October 1968. (NWC TP 4630).

4. Princeton University, Department of Aeronautical Engineering. Modification of the Burning Rates of Ammonium Perchlorate Solid Propellants, by E. K. Bastress. Princeton, N. J., Princeton Univ., March 1961. (Aeronautical Engineering Report No. 536, under Contract Nonr-1858(32)-NR 098-201).

5. Bastress, E. K., K. P. Hall, and M. Summerfield. Modification of the Burning Rates of Solid Propellants by Oxidizer Particle Size Control. New York, American Rocket Society, 1961. (ARS Preprint.)

6. Steinz, J. A., P. L. Stand, and M. Summerfield. "The Burning Mechanism of Ammonium Perchlorate-Based Composite Solid Propellants," in "ICRPG/AIAA 3rd Solid Propulsion Conference." Atlantic City, N. J., AIAA, June 1968. Preprint No. 68-658.

7. Army Research and Development Group (Europe). The Prediction of the Burning Rate Exponent of Solid Propellants, by Robert J. Heaston. New York, N. Y., ARDG, December 1966. (DDC Document AD 815882.)

8. Summerfield, M., G. S. Sutherland, M. J. Webb, H. J. Taback, and K. P. Hall. "Burning Mechanism of Ammonium Perchlorate Propellants, Solid Propellant Rocket Research," in PROG ASTRON ROCKETRY, Vol. 1 (1960), pp. 141-82.

9. Krier, H., H. B. Mathes, E. W. Price, and M. Summerfield. "Entropy Waves Produced in Oscillatory Combustion of Solid Propellants," in "ICRPG/AIAA 3rd Solid Propulsion Conference." New York, N. Y., AIAA, 1968. Preprint No. 68-499.

UNCLASSIFIED
Security Classification

DOCUMENT CONTROL DATA - R&D		
(Security classification of title, body of abstract and indexing annotation must be entered when the overall report is classified)		
1 ORIGINATING ACTIVITY (Corporate author) Naval Weapons Center China Lake, California		2a REPORT SECURITY CLASSIFICATION UNCLASSIFIED; 2b GROUP
3 REPORT TITLE LOW-FREQUENCY COMBUSTION INSTABILITY PROGRESS REPORT 1 OCTOBER 1967-31 MARCH 1968		
4 DESCRIPTIVE NOTES (Type of report and inclusive dates) Research Report		
5 AUTHOR(S) (Last name, first name, initial) Mathes, H. B., Boggs, T. L., Dehority, G. L., Crump, J. E.		
6. REPORT DATE December 1968	7a. TOTAL NO. OF PAGES 44	7b NO. OF REFS 9
8a. CONTRACT OR GRANT NO / b PROJECT NO. / c NASA Work Order 6030 / d.	9a. ORIGINATOR'S REPORT NUMBER(S) NWC TP 4565; 9b. OTHER REPORT NO(S) (Any other numbers that may be assigned this report)	
10 AVAILABILITY/LIMITATION NOTICES This document is subject to special export controls and each transmittal to foreign governments or foreign nationals may be made only with prior approval of the Naval Weapons Center.		
11. SUPPLEMENTARY NOTES	12. SPONSORING MILITARY ACTIVITY Naval Air Systems Command Naval Materials Command Washington, D. C. 20360	

13. ABSTRACT

This ~~semiannual~~ report summarizes studies of the burning rate of composite propellants, acoustic and nonacoustic low-frequency combustion instability of composite propellants and nonisentropic combustion behavior in T-burners.

DD FORM 1 JAN 64 1473 0101-807-6800

UNCLASSIFIED
Security Classification

UNCLASSIFIED
Security Classification

14 KEY WORDS	LINK A ROLE	LINK A WT	LINK B ROLE	LINK B WT	LINK C ROLE	LINK C WT
Combustion instability						
Solid propellants						
Polyurethane binder						
Carboxy-terminated polybutadiene binder						
Burning rate						
Granular Diffusion Flame model						
Gas behavior						
T-burner						
Computer program						

INSTRUCTIONS

1. ORIGINATING ACTIVITY: Enter the name and address of the contractor, subcontractor, grantee, Department of Defense activity or other organization *(corporate author)* issuing the report.

2a. REPORT SECURITY CLASSIFICATION. Enter the overall security classification of the report. Indicate whether "Restricted Data" is included. Marking is to be in accordance with appropriate security regulations.

2b. GROUP: Automatic downgrading is specified in DoD Directive 5200.10 and Armed Forces Industrial Manual. Enter the group number. Also, when applicable, show that optional markings have been used for Group 3 and Group 4 as authorized.

3. REPORT TITLE: Enter the complete report title in all capital letters. Titles in all cases should be unclassified. If a meaningful title cannot be selected without classification, show title classification in all capitals in parenthesis immediately following the title.

4. DESCRIPTIVE NOTES: If appropriate, enter the type of report, e.g., interim, progress, summary, annual, or final. Give the inclusive dates when a specific reporting period is covered.

5. AUTHOR(S): Enter the name(s) of author(s) as shown on or in the report. Enter last name, first name, middle initial. If military, show rank and branch of service. The name of the principal author is an absolute minimum requirement.

6. REPORT DATE. Enter the date of the report as day, month, year, or month, year. If more than one date appears on the report, use date of publication.

7a. TOTAL NUMBER OF PAGES: The total page count should follow normal pagination procedures, i.e., enter the number of pages containing information.

7b. NUMBER OF REFERENCES: Enter the total number of references cited in the report.

8a. CONTRACT OR GRANT NUMBER: If appropriate, enter the applicable number of the contract or grant under which the report was written.

8b, 8c, & 8d. PROJECT NUMBER: Enter the appropriate military department identification, such as project number, subproject number, system numbers, task number, etc.

9a. ORIGINATOR'S REPORT NUMBER(S): Enter the official report number by which the document will be identified and controlled by the originating activity. This number must be unique to this report.

9b. OTHER REPORT NUMBER(S): If the report has been assigned any other report numbers *(either by the originator or by the sponsor)*, also enter this number(s).

10. AVAILABILITY/LIMITATION NOTICES: Enter any limitations on further dissemination of the report, other than those imposed by security classification, using standard statements such as:

(1) "Qualified requesters may obtain copies of this report from DDC."

(2) "Foreign announcement and dissemination of this report by DDC is not authorized."

(3) "U. S. Government agencies may obtain copies of this report directly from DDC. Other qualified DDC users shall request through ________________."

(4) "U. S. military agencies may obtain copies of this report directly from DDC. Other qualified users shall request through ________________."

(5) "All distribution of this report is controlled. Qualified DDC users shall request through ________________."

If the report has been furnished to the Office of Technical Services, Department of Commerce, for sale to the public, indicate this fact and enter the price, if known.

11. SUPPLEMENTARY NOTES: Use for additional explanatory notes.

12. SPONSORING MILITARY ACTIVITY: Enter the name of the departmental project office or laboratory sponsoring *(paying for)* the research and development. Include address.

13. ABSTRACT: Enter an abstract giving a brief and factual summary of the document indicative of the report, even though it may also appear elsewhere in the body of the technical report. If additional space is required, a continuation sheet shall be attached.

It is highly desirable that the abstract of classified reports be unclassified. Each paragraph of the abstract shall end with an indication of the military security classification of the information in the paragraph, represented as *(TS)*, *(S)*, *(C)*, or *(U)*.

There is no limitation on the length of the abstract. However, the suggested length is from 150 to 225 words.

14. KEY WORDS: Key words are technically meaningful terms or short phrases that characterize a report and may be used as index entries for cataloging the report. Key words must be selected so that no security classification is required. Identifiers, such as equipment model designation, trade name, military project code name, geographic location, may be used as key words but will be followed by an indication of technical context. The assignment of links, roles, and weights is optional.

UNCLASSIFIED
Security Classification